Influence of sea surface temperature patterns and mean warming on past and future Atlantic hurricane activity

E. L. Levin[a] G. A. Vecchi,[b] W. Yang,[b]

[a] *Program in Atmospheric and Oceanic Sciences, Princeton University*

[b] *Department of Geosciences, Princeton University*

Corresponding author: Emma Levin, emma.levin@princeton.edu

ABSTRACT: This study investigates the relative contributions of large-scale thermodynamic and dynamic processes to multidecadal changes in Atlantic tropical cyclone (TC) activity, spanning the historical record since the late 19th century, and extending to 2100 projections. We employ a framework that decomposes TC counts into precursor disturbances that transition into fully developed storms, applied to multi-ensemble simulations of two TC-permitting atmospheric models forced with observationally-constrained and projected sea surface temperatures (SSTs). This design allows us to isolate the effects of patterns of SST change from global mean warming on Atlantic TC activity. Our results show that multidecadal trends in TC frequency are primarily governed by two thermodynamic variables: potential intensity and moist entropy deficit. In the historical record, these variables reinforced one another, producing more robust trends in TC activity. In contrast, future projections suggest opposing influences, with one variable (potential intensity) becoming more favorable for TCs while the other (moist entropy deficit) becomes less favorable, leading to increased uncertainty in TC projections. We trace this shift to differences in relative warming between the tropical Atlantic and the broader tropics, underscoring that regional SST patterns—rather than the global mean warming rate—control both past variability and projected future changes in TC activity. Constraining future patterns of warming is therefore essential for improving the reliability of TC projections.

1. Introduction

Responsible for over $250 billion of inflation-adjusted losses in the U.S. between 2008 and 2017 (Klotzbach et al. (2018)), landfalling tropical cyclones (TCs) that form in the Atlantic Ocean are a major hazard for both coastal and inland communities in the U.S. and Caribbean. Further, it is crucial to understand the factors that have driven past fluctuations in Atlantic storm activity, and the extent to which anthropogenic warming might influence TCs in the future.

While several studies attempting to reconstruct a reliable historical record of Atlantic TCs generally disagree on the direction of the trend in Atlantic TC counts from the late-19th century to the present (Emanuel (2021a),Vecchi and Knutson (2008), Vecchi and Knutson (2011), Vecchi et al. (2021)), they attribute past fluctuations in seasonal storm frequency to regional climate variability, warming patterns, and aerosol concentrations, rather than global anthropogenic warming. For instance, several studies indicate that natural climate modes, such as the Atlantic Multi-decadal Oscillation (Goldenberg et al. (2001); Klotzbach (2011b); Zhang and Delworth (2006)) and the El Niño Southern Oscillation (Klotzbach (2011a); Klotzbach et al. (2022); Patricola et al. (2016); Pielke and Landsea (1999); Xie et al. (2005)), along with their corresponding oscillating sea surface temperature patterns, can influence North Atlantic TC activity.

Although there is a growing consensus that global warming contributes to an increase in peak TC windspeed and rainfall intensity (see reviews Knutson et al. (2020) and Walsh et al. (2019) and references therein), it remains unclear how seasonal TC counts will change in a warmer world (Knutson et al. (2020) and Sobel et al. (2021)). Most studies based on climate model simulations project a decrease or minimal change in global TC count (see reviews Knutson et al. (2020) and Walsh et al. (2019) and references therein). However, some modeling studies (e.g., Bhatia et al. (2018), Vecchi et al. (2019)) and statistical-dynamical downscaling efforts (e.g., Emanuel (2013), Emanuel (2021b)) predict an increase in TC frequency due to anthropogenic global warming.

Several factors may explain the discrepancies in TC frequency projections across studies. First, these studies use various climate models with differing parametrization schemes and horizontal resolutions, ranging from tens to hundreds of kilometers, that may or may not resolve TCs and mesoscale processes (Camargo et al. (2020); Hsieh et al. (2023); Manganello et al. (2012)). Inconsistencies in TC projections may also stem from uncertainties regarding the impact of thermodynamic variables, particularly humidity, on TC genesis. For instance, saturation deficit represents the difference between the specific humidity of the atmosphere and its specific humidity at saturation (Olszewski (1986)). In a warmer world, the saturation deficit in the lower and mid-troposphere increases (Held and Soden (2000); Emanuel (2010, 2021a)). A higher saturation deficit would require an increased surface moisture flux to bring the atmospheric column to saturation, which could inhibit deep convection and cyclogenesis (Sobel et al. (2021), Tang and Camargo (2014)). This theory suggests that with a higher saturation deficit in a warmer world, TC activity would decrease (Camargo et al. (2014); Emanuel (2021a); Emanuel (2010); Lee et al. (2020); Lee et al. (2023); Vecchi et al. (2019)). However, several high-resolution models project an increase in TC activity (Bhatia et al. (2018); Vecchi et al. (2019)), despite a rise in saturation deficit. These studies suggest that the interplay between local thermodynamic and dynamic variables could play an important role in driving changes in TC activity. In the models that show a TC frequency increase, the reduced genesis favorability from changes in saturation is outweighed by an increase in pre-TC vortices ('seeds') (Vecchi et al. 2019; Hsieh et al. 2020).

Finally, inherent model biases and variations in projections of regional climate and sea surface temperature (SST) patterns, particularly in the Eastern Pacific and Atlantic basins (see review by Shaw et al. (2024) and references therein), could lead to differences in future TC projections. Atlantic TCs are sensitive to the relative average temperature of the tropical Atlantic compared to the rest of the tropics (Vecchi and Soden (2007); Villarini et al. (2011b)).

To investigate the relationships between large-scale environmental factors and TC activity, several indices have been developed (e.g., Bruyère et al. (2012); Emanuel and Nolan (2004); Emanuel (2010); Tippett et al. (2011); Wang and Murakami (2020)). These indices, known as genesis potential indices (GPIs), relate local environmental factors—such as potential intensity (PI), vertical wind shear, and humidity—to TC activity. GPIs are typically calculated from monthly averages, representing regional climatology rather than instantaneous weather conditions (Sobel et al. (2021)). While GPIs have been used to predict the effects of future climate change on TC activity (e.g., Murakami and Wang (2022)), Camargo et al. (2014) found that most GPIs fail to capture future TC projections from atmosphere-only climate models.

As an alternative way to construct GPIs, Hsieh et al. (2020) present a framework for understanding how large-scale local environmental fields influence TC formation. Unlike traditional GPIs (Emanuel (2022)), this approach divides tropical cyclogenesis into distinct phases, identifying the specific large-scale local factors relevant to each stage of TC development. This framework is motivated by a recognition that the feedbacks on development of TCs are different at different stages (Hsieh et al. 2020; Zhang et al. 2021), and thus the environmental controls on seeds and the likelihood of genesis to a mature TC may be different. This technique of separating TCs into seeds and a nondimensional probability that a seed transitions into a TC has proven useful for studying TCs across various timescales, including their annual cycle (Yang et al. (2021)) and over longer idealized climatic periods (Hsieh et al. (2022); Hsieh et al. (2023); Vecchi et al. (2019)). In this study, we extend the application of this framework to the long observed historical record, where it has not yet been applied. Additionally, we focus this approach on the Atlantic basin, where seed-like disturbances may be influenced by nonlocal factors, such as African Easterly Waves (Patricola et al. (2018), Ritchie and Holland (1999)).

Through this work, we aim to address the following research questions:

1. To what extent does the theoretical framework proposed by Hsieh et al. (2020) capture long-term observed and projected regional Atlantic TC variability?

2. To what extent do different environmental factors (both thermodynamic and dynamic) modulate Atlantic TCs in the observed and projected records, and how are these factors related to regional warming patterns versus globally-uniform warming?

To address these questions, we employ the seed-probability framework within a suite of state-of-the-art high-resolution atmosphere-only general circulation model experiments that have demonstrated skill in simulating key characteristics of past TC activity (Chan et al. (2021), Chen and Lin (2011), Zhao et al. (2009), and Zhao and Held (2010)). We seek to identify the dominant large-scale environmental factors driving historical and future projected variations in Atlantic TC frequency. By utilizing atmosphere-only models forced by observed SSTs, we effectively isolate the influence SST patterns on TC activity.

2. Methods and data

a. Models and experiments

In this study, we employ two closely related global high-resolution atmospheric models from the Geophysical Fluid Dynamics Laboratory (GFDL): AM2.5-C360 and HIRAM (Zhao et al. (2009)), both of which have been used to study tropical cyclones (TCs). These models share the same dynamical core but differ in their convection parameterizations and horizontal resolutions. AM2.5-C360 uses the relaxed Arakawa–Schubert convective parametrization scheme, while HIRAM uses the parametrization method described in Bretherton et al. (2004). HIRAM, with a horizontal resolution of 50 km, has demonstrated skill in simulating various aspects of past TC variability (Chen and Lin (2011), Zhao et al. (2009), and Zhao and Held (2010)). AM2.5-C360, on the other hand, has a higher resolution of 25 km, and has been employed in prior studies to examine the influence of SSTs on tropical cyclone activity (Chan et al. 2021), the annual cycle of TCs (Yang et al. 2021), and the evolution of storm tracks under warming conditions (Kortum et al. 2024). The use of atmosphere-only models forced with prescribed SSTs provides a clean framework for isolating the role of SST patterns in shaping TC behavior.

We conducted two multi-ensemble experiments with both models to capture historical and future climate scenarios. For the first experiment, hereafter named *obs sst*, we generated ten ensemble members of AM2.5-C360 and five ensemble members of HIRAM, all forced by bias-corrected observed sea surface temperatures (Chan et al. (2021)) from the Hadley Centre Sea Ice and Sea Surface Temperature (HADISST) dataset for the period 1871–2020. Each ensemble member was initialized with different initial conditions but used the same historical SST forcing.

The second experiment represents a projected late 21st-century warming scenario. The SST perturbation for this experiment, hereafter referred to as *rcp4.5 flor*, consists of six ensemble members of AM2.5-C360 and three ensemble members of HIRAM. The three ensembles of HIRAM and first three ensembles of AM2.5-C360 are forced with ensemble-mean 2021-2100 SST from the GFDL Forecast-oriented Low Ocean Resolution (FLOR) RCP4.5 coupled model experiment, while the last three ensembles of AM2.5-C360 are forced with 2021-2100 SSTs from the first ensemble member of FLOR RCP4.5 experiment. This configuration represents the model's realization of future climate variability. The FLOR model (Vecchi et al. (2014)) features an ocean model with an approximately $1^\circ \times 1^\circ$ ocean spatial resolution, and an atmospheric model with the same physics and dynamical core as AM2.5-C360, but run at a lower atmospheric spatial resolution of approximately 50 km.

b. Data

For the historical record of Atlantic tropical cyclone (TC) frequencies from 1871 to 2020, we utilize the adjusted dataset developed by Vecchi and Knutson (2008). To compute observed seasonal large-scale environmental factors, we use the ERA5 reanalysis dataset (Hersbach et al. 2020) during the period 1979–2020 and the MERRA2 reanalysis dataset (Gelaro et al. 2017) during the period 1980-2020.

c. TC and seed tracking

To track tropical cyclones (TCs), we employ the algorithm developed by Harris et al. (2016), setting the specific thresholds for wind speed, minimum sea level pressure, lifetime, and warm-core characteristics as in Chan et al. (2021). The algorithm utilizes the following 6-hourly inputs: sea level pressure, 850 hPa vorticity, 10-m wind speed, and mid-tropospheric (300–500 hPa) air temperature. The process begins by searching for local minima in sea level pressure and then applying an 850 hPa vorticity threshold of $1.5 \times 10^{-4} \mathrm{s}^{-1}$, which filters out disorganized or weak systems. For the remaining storms, additional filters ensure longevity and robustness, including a minimum total lifetime of 72 hours (Villarini et al. (2011a)), at least 48 hours with a warm core (defined as a maximum 300–500 hPa temperature encircled by a 2° contour within 500 km of the storm's minimum sea level pressure), and at least 36 consecutive hours with both a warm core and maximum 10-m winds exceeding 15 m s^{-1}. We require that at least one time step along the storm's trajectory that the maximum wind speed exceeds 17 m s^{-1}.

For the HIRAM model, we make slight adjustments to this algorithm. The warm-core temperature contour is increased from 2 to 2.5° and the required proximity of the warm core to the storm center is decreased from 500 km to 110 km. For the AM2.5-C360 model, we retain the original thresholds without modifications.

Seed detection is performed using the aforementioned TC tracking algorithm, with the approach described in Yang et al. (2021). We examine candidate points as local pressure minimal that exceed the a $1.5 \times 10^{-4} \mathrm{s}^{-1}$ vorticity threshold. A seed must span a radius of at least 50 km and exhibit a maximum 850 hPa relative vorticity of at least $4 \times 10^{-4} \mathrm{s}^{-1}$ during its lifetime. The seed tracking algorithm remains unchanged for both atmospheric models.

d. Seed and probability indices

We use Hsieh et al. (2020)'s probabilistic framework, which decomposes annual TC counts into two stages: precursor seed disturbances and fully developed TCs. Based on these two stages, Hsieh et al. (2020) infer that the annual frequency of North Atlantic TCs, N_{TC} follows a binomial distribution:

$$N_{TC} \sim \text{binom}(N_s, P), \tag{1}$$

where N_s is the total number of first stage rotating seeds present in the basin for a given year, which has units of storm count, and P is the dimensionless basin-aggregated probability that a first-stage seed transitions into a second-stage TC. Consequently, the expected value of N_{TC}, which has dimensions of storm count, is given by

$$N_{TC} = N_s \times P. \tag{2}$$

For instance, if a given season produces 75 seeds ($N_s = 75$), of which 15 transition into TCs ($N_{TC=15}$), the basin-aggregated transition probability from the first stage to the second stage for that season would be $P = 15/75 = 0.2$.

Hsieh et al. (2020)'s ansatz parametrizes N_s and P as functions of large-scale environmental conditions. First, they develop a proxy for N_s, known as the seed propensity index (SPI):

$$N_s \approx SPI = (\kappa) \cdot (-\omega) \cdot \frac{1}{1 + Z^{-1/\sigma}}, \tag{3}$$

where κ is a constant proportionality fitted parameter in units of storms per Pa s^{-1}, ω is the monthly mean 500 hPa vertical velocity in pressure coordinates (in units of Pa s^{-1} where $\omega > 0$ is for downward motion), $\sigma = 0.69$ is a constant nondimensional fitting parameter, and Z is nondimensional parameter that represents the ability of the low-level vorticity to spinup and is a function of low level vorticity (Ikehata and Satoh (2021)),

$$Z = \frac{f + \zeta}{\sqrt{|\beta + \partial_y \zeta| U}}, \tag{4}$$

where f represents the Coriolis parameter and β represents its meridional gradient, ζ is the monthly mean relative vorticity at 850 hPa, and U is assumed to be a constant wind speed of 20 m/s which is empirically fit using aquaplanet model simulations.

Next, the probability that a weakly rotating seed develops into a strongly rotating TC (P; a dimensionless value between 0 and 1) is parameterized as a probability index ($P(\Lambda)$):

$$P \approx P(\Lambda) = \frac{1}{1 + (\Lambda_0/\Lambda)^{1/\gamma}}, \tag{5}$$

where $\Lambda_0 = 0.014$ and $\gamma = -0.9$ are constant dimensionless fitting parameters, and Λ is the ventilation index defined by Tang and Emanuel (2010) and Tang and Emanuel (2012), which measures the degree to which the influx and circulation of cold dry air into the storm's convective plume can inhibit the storm's strength. The ventilation index is a non-dimensional metric:

$$\Lambda = \frac{v_s \cdot \chi}{PI}, \tag{6}$$

where v_s is the vertical wind shear between 850 hPa and 250 hPa in units of m s^{-1}, PI is potential intensity (the theoretical upper limit of a TC's wind speed based on temperature contrasts between the sea surface and upper troposphere in units of m s^{-1}), and χ is a dimensionless parameter representing moist entropy deficit. This parameter is defined as

$$\chi = \frac{s_m^* - s_m}{s_0^* - s_b}, \tag{7}$$

where s_m^* is the saturation moist entropies at 600 hPa in the inner core of a TC, s_m is the environmental entropy at 600 hPA, s_0^* are the saturation moist entropy at the sea surface, and s_b is the entropy of the boundary layer. The numerator of the ventilation index equation (6) represents the difference in midlevel entropy between the TC and its environment, while the denominator represents the air-sea disequilibrium.

Thus, equations (3) and (5) serve as proxies for N_s and P expressed as functions of large-scale environmental factors that can be derived from climate model simulations. This framework offers a valuable approach for studying TCs using climate models, particularly those that lack the spatial resolution required to directly resolve TCs and seeds. We compute the mean annual Atlantic basin SPI between 5-30°N and $P(\Lambda)$ between 10-30°N for TC season (June-November).

3. Results

a. Evaluating the models and seed-probability framework for Atlantic TCs

In this section, we evaluate the extent to which the seed-probability framework captures both historical and projected TC variability in our model simulations. We begin by assessing how well the simulations reproduce historical observed TC variability. Figure 1a compares observed annual Atlantic TC counts to those simulated by both models. Overall, both simulations effectively capture interannual fluctuations in TC activity. For instance, both models simulate a local peak in 2005 and a trough in 1982, corresponding to historically active and inactive years, respectively. The annual ensemble-mean correlation between simulated and observed TC frequency is slightly higher in AM2.5-C360 compared to HIRAM, though both exhibit similar values (~0.5).

For most years, observed TC fluctuations (black line) remain within the 95% inter-ensemble spread of both models (blue and orange shading), suggesting that the models reproduce realistic levels of TC variability. However, the exceptionally active 2020 season, and several seasons immediately preceding it, are not well captured, with observed TC counts lying outside the 95% confidence interval of both models. Work is better underway to better understand the extent to which this discrepancy, which represents a deficiency in the models or the forcing, is due to ambiguity in the observed target or is likely to be best understood as one of the unlikely outcomes that even a well-calibrated system will exhibit.

We propose several hypotheses for this model–observation discrepancy. First, aerosol changes during this period may not have been fully represented in the SST-forced simulations. The onset of the COVID-19 pandemic in early 2020 sharply reduced global travel and industrial activity, likely lowering aerosol emissions. At the same time, new International Maritime Organization regulations, effective January 1, 2020, reduced the sulfur content of shipping fuels from 3.5% to 0.5%. While intended to improve air quality and public health, this reduction diminished marine aerosol loading, brightening fewer clouds and decreasing reflected solar radiation. The resulting radiative imbalance likely accelerated short-term warming, creating atmospheric conditions more

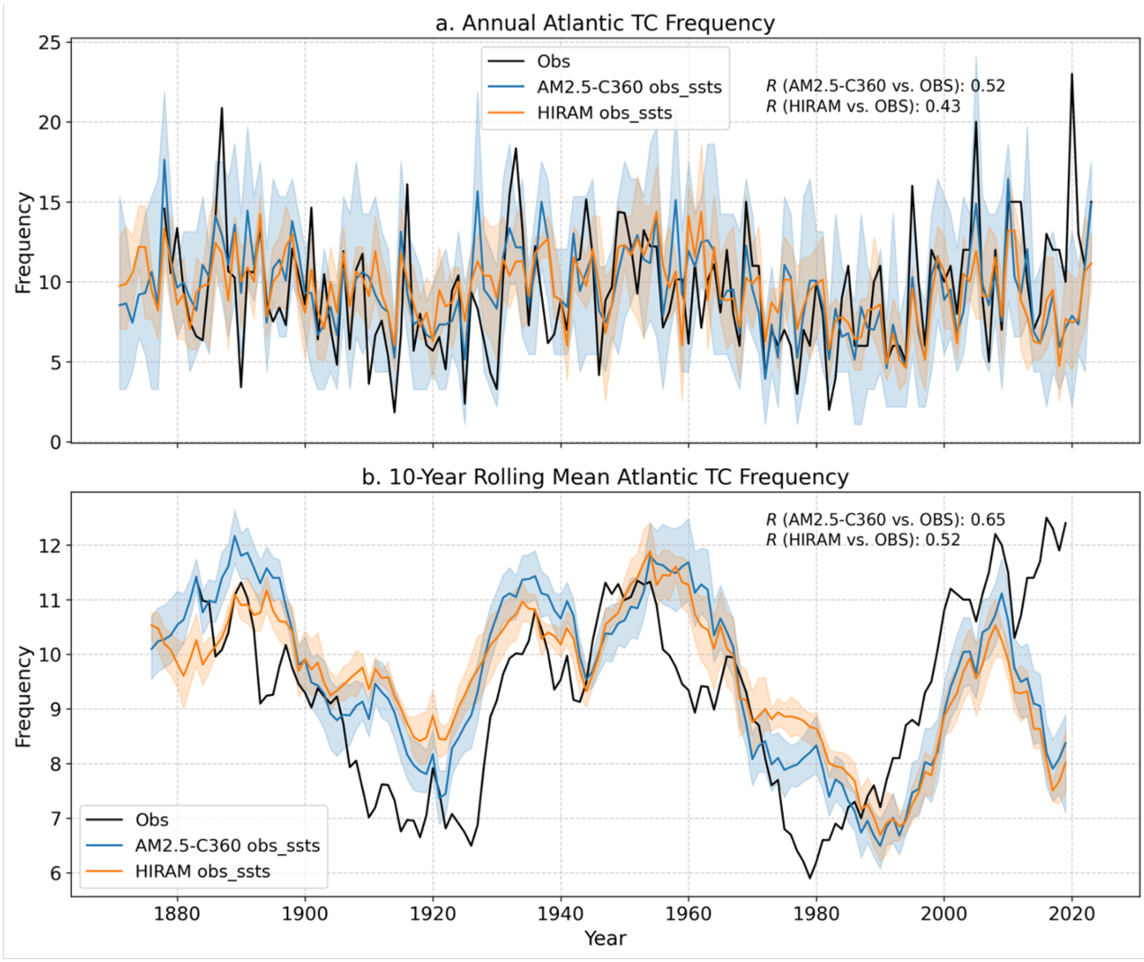

FIG. 1. Annual TC frequency from 1871 to 2023, including the adjusted observational record from Vecchi and Knutson (2011) (black), AM2.5-C360 obs_sst simulation (blue), and HIRAM obs_sst simulation (orange). Here, the model shading represents the bootstrapped 95% confidence interval derived from resampled ensemble members for each model, while the solid lines indicate the ensemble means. (b) The 10-year rolling mean of the TC frequency data shown in (a).

favorable for TC development (Diamond 2023; Jordan and Henry 2024; Zhang et al. 2025). Still, such effects cannot account for the discrepancies observed in the years immediately prior to 2020.

Additional possile causes include model and storm-tracking limitations within AM2.5-C360 and HIRAM, as well as evolving observational practices since the advent of the satellite era. For example, modern satellites may have become increasingly capable of detecting weaker disturbances, inflating the observed storm record relative to earlier periods. Finally, internal climate variability and random weather fluctuations may also have played a role (Kortum et al. 2024). A fuller exploration of these hypotheses lies beyond the scope of this report but remains an important direction for future research.

Figure 1b evaluates the models' ability to capture past decadal variability in Atlantic TC activity using a 10-year rolling mean. Both models successfully reproduce distinct multi-decadal fluctuations observed since the 19th century, as was discussed in Chan et al. (2021). For example, they capture peaks in the 1950s and early 2000s, as well as troughs in the 1920s and 1980s.

As in the annual analysis, the ensemble spread is larger in AM2.5-C360, and the ensemble-mean correlation coefficient is slightly higher in this model. Notably, the correlation coefficients for the 10-year rolling mean are slightly improved compared to those for annual TC frequencies, suggesting that the models perform better at capturing long-term variability. However, a clear discrepancy emerges in the 2010s, primarily due to the models' inability to replicate the highly active 2020 season and its few preceding seasons.

b. Evolution of TC seed and probability proxies

To understand the drivers of the TC activity changes, we examine the correlation between the parametrized TC estimate ($SPI \times P(\Lambda)$) and the simulated TCs from the models. It is important to note that the proxies SPI and $P(\Lambda)$ are not indepenent variables, but exhibit a spatial-temporal covariation (A1). Visual inspection of Fig. 2 suggests that the framework effectively captures decadal TC variability in both models across the historical and projected periods. For instance, in both models, the framework identifies peaks in TC activity around 1890 and 1950, as well as troughs around 1920 and 1980. Similarly, it captures projected variability, with peaks aligning in 2050 and 2070 and a trough in 2060.

In both observed and projected periods, the parametrized TCs remain within the 95% confidence interval of the simulated TCs, indicating that the framework provides a realistic representation of TC variability. However, when comparing model performance, the framework exhibits stronger agreement with HIRAM than AM2.5-C360, as reflected in the higher correlation coefficient between parametrized and simulated ensemble mean TC count (0.94 vs. 0.78). Notably, the framework underestimates projected TC activity in AM2.5-C360, while in both models, it overestimates peaks in 1950 and 1990 during the historical period.

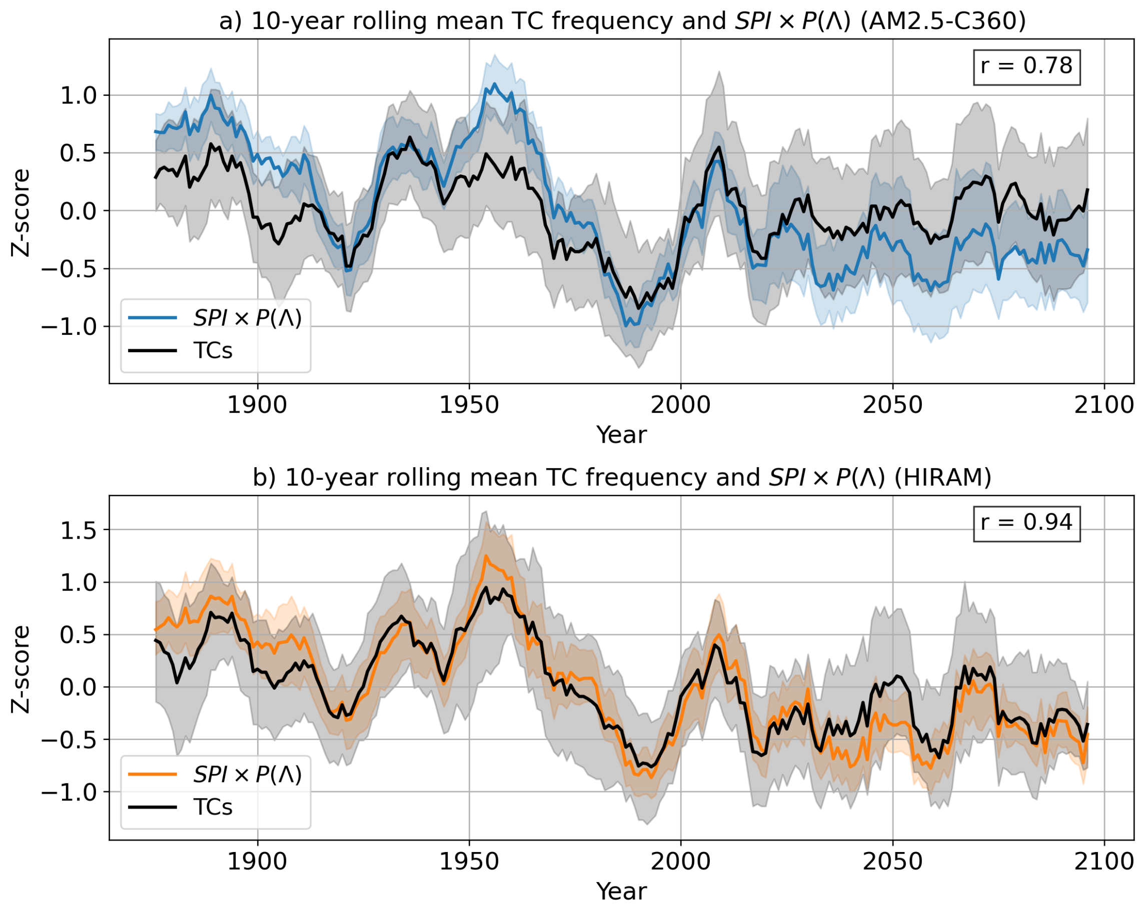

FIG. 2. Normalized 10-year rolling mean of simulated Atlantic tropical cyclone (TC) frequency (N_{TC}; black) and parameterized TC frequency (SPI $\times P(\Lambda)$; colored) for (a) AM2.5-C350 (blue) and (b) HIRAM (orange). Shaded regions indicate the bootstrapped 95% confidence intervals, derived from resampled ensemble members, while solid lines represent the ensemble means. The historical period (1871–2019) is based on the <u>*obs SST*</u> simulation, whereas the future period (2020–2100) is derived from the <u>*rcp4.5 SST*</u> simulation. These two periods are combined into a continuous time series, with both simulated and parameterized TC frequencies standardized using a Z-score normalization: $Z(x) = (x - \mu_x)/\sigma_x$, where x represents the data point, μ_x is the mean, and σ_x is the standard deviation over the full record. Correlation coefficients between the ensemble mean simulated and parameterized TC frequencies are displayed in the top right corner of each panel.

Next, we assess the variability of SPI, $P(\Lambda)$, and their contributing variables in both historical and projected records. Figure 3 illustrates the temporal evolution of SPI and $P(\Lambda)$ across the entire combined record in both model simulations. Notably, the models exhibit distinct magnitudes of

SPI and $P(\Lambda)$, with $P(\Lambda)$ consistently higher in AM2.5-C360 than in HIRAM by approximately 0.1, while SPI remains lower in AM2.5-C360 by about 1.5×10^{-3}. Examining SPI in Figure 3b, we find no discernible long-term trend but rather multidecadal and decadal variability. During the historical period (1871–2019), SPI displays prominent multidecadal fluctuations, with peaks in the 1880s–1890s and 1940s–1950s, and troughs in the 1920s–1930s and 1980s–1990s. In contrast, the projected record reveals predominantly decadal variability, characterized by peaks recurring approximately every 20 years. Meanwhile, $P(\Lambda)$ follows a distinct pattern: during the historical period, it exhibits a steady decline before stabilizing in the projected record, where variability remains relatively stagnant. The most striking trend in the entire record for both SPI and $P(\Lambda)$ is a is a sharp decline from 1950 to 1980, followed by a notable rebound and increase from 1980 to 2010.

(i) Thermodynamic variables

To understand why $P(\Lambda)$ exhibits a decreasing trend throughout the historical period but remains relatively stable in the projected period, we examine its thermodynamic components, χ and PI, both of which respond directly to anthropogenic warming. Figure 4 illustrates the relationship between PI and χ^{-1} in both the historical and projected model simulations, as well as in several reanalysis datasets. During the historical period (blue) and across the duration of the reanalysis data (orange and olive), we observe a direct relationship between PI and χ^{-1}, indicating that their effects compounded each other. When PI was higher and more conducive to tropical cyclones (TCs), χ was lower, further enhancing storm activity. In contrast, during the projected period (green), this relationship reverses: as one variable becomes more favorable for TC activity, the other becomes less favorable, suggesting that their effects offset each other. Additionally, the models exhibit distinct magnitudes of PI and χ^{-1}. PI is notably higher in HIRAM by approximately 7 m s^{-1}. While PI values in HIRAM are closer to those found in reanalysis products, they still fall short by about 5 m s^{-1}. Meanwhile, χ^{-1} is slightly higher in AM2.5-C360 than in HIRAM, though the reanalysis datasets display significant variation in their projections of χ^{-1}.

To further investigate the reversal of the relationship between χ and PI in the historical and projected periods, we plot their time series in Figure 5. The results show that χ increases consistently throughout the entire record, suggesting that anthropogenic warming enhances the moisture deficit between the storm's inner core and its environment. Meanwhile, the trend lines

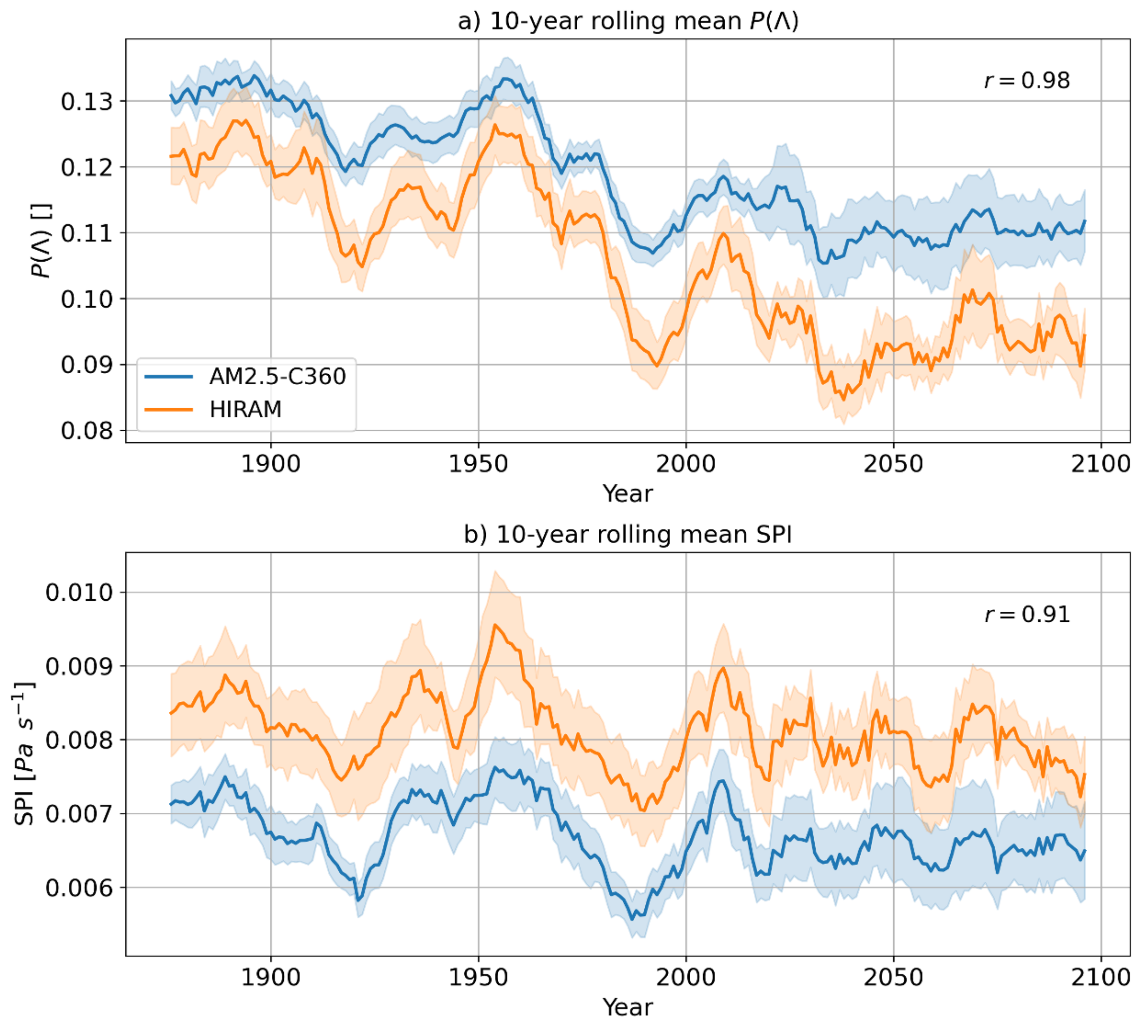

FIG. 3. 10-year rolling mean of a) $P(\Lambda)$ and b) SPI, from AM2.5-C360 (blue) and HIRAM (orange). Shaded regions indicate the bootstrapped 95% confidence intervals, derived from resampled ensemble members, while solid lines represent the ensemble means. The historical period (1871–2019) is based on the *obs SST* simulation, whereas the future period (2020–2100) is derived from the *rcp4.5 SST* simulation. These two periods are combined into a continuous time series. The correlation coefficients between the ensemble mean of each model is shown in the upper right corner of each panel.

in Figure 5 reveal that PI decreases throughout the historical period but increases in the projected period. This shift in the sign of the PI trend is the primary driver of the observed reversal in the PI and χ relationship.

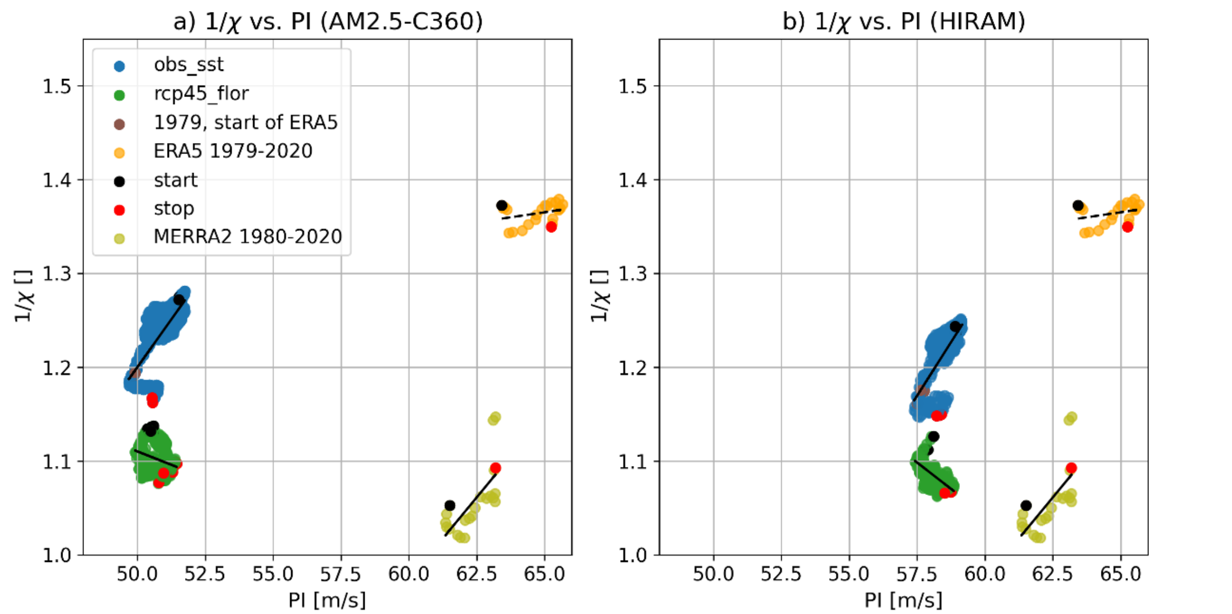

FIG. 4. 10-year rolling mean of TC-season basin-averaged χ^{-1} and PI for (a) AM2.5-C360 and (b) HIRAM. To clarify their relationship, both axes are oriented so that increasing values indicate more favorable conditions for TC activity. Blue and green dots represent historical (1871–2019) and projected (2020–2100) periods, respectively, while orange and olive dots correspond to ERA5 (1979–2020) and MERRA5 (1980–2020) reanalysis data. Black and red dots denote the start and end of each period. Trend lines are plotted for each period, with solid lines indicating statistically significant trends ($p < 0.05$) and dashed lines otherwise. Positive (negative) trends indicate periods where PI and χ effects reinforce (offset) each other.

To better understand the discrepancy between observed and projected trends in PI, we analyze trends in tropical sea surface temperatures (SSTs) during both periods. Tropical SSTs exert a strong influence on upper-tropospheric temperatures, which in turn regulate PI (Emanuel et al. (2013); Eusebi et al. (2025); Ramsay and Sobel (2011); Vecchi and Soden (2007); Vecchi et al. (2013)), since PI is fundamentally determined by the temperature contrast between the surface and the upper troposphere. The primary mechanism linking SSTs to free-tropospheric temperatures is deep convection (Flannaghan et al. (2014); Fueglistaler et al. (2015); Sobel et al. (2002)), which is most vigorous in regions of the warmest tropical SSTs (Zhang (1993)). Consequently, the warmest tropical SSTs—typically associated with the western Pacific warm pool—effectively set upper-tropospheric temperatures across the tropics through convective adjustment.

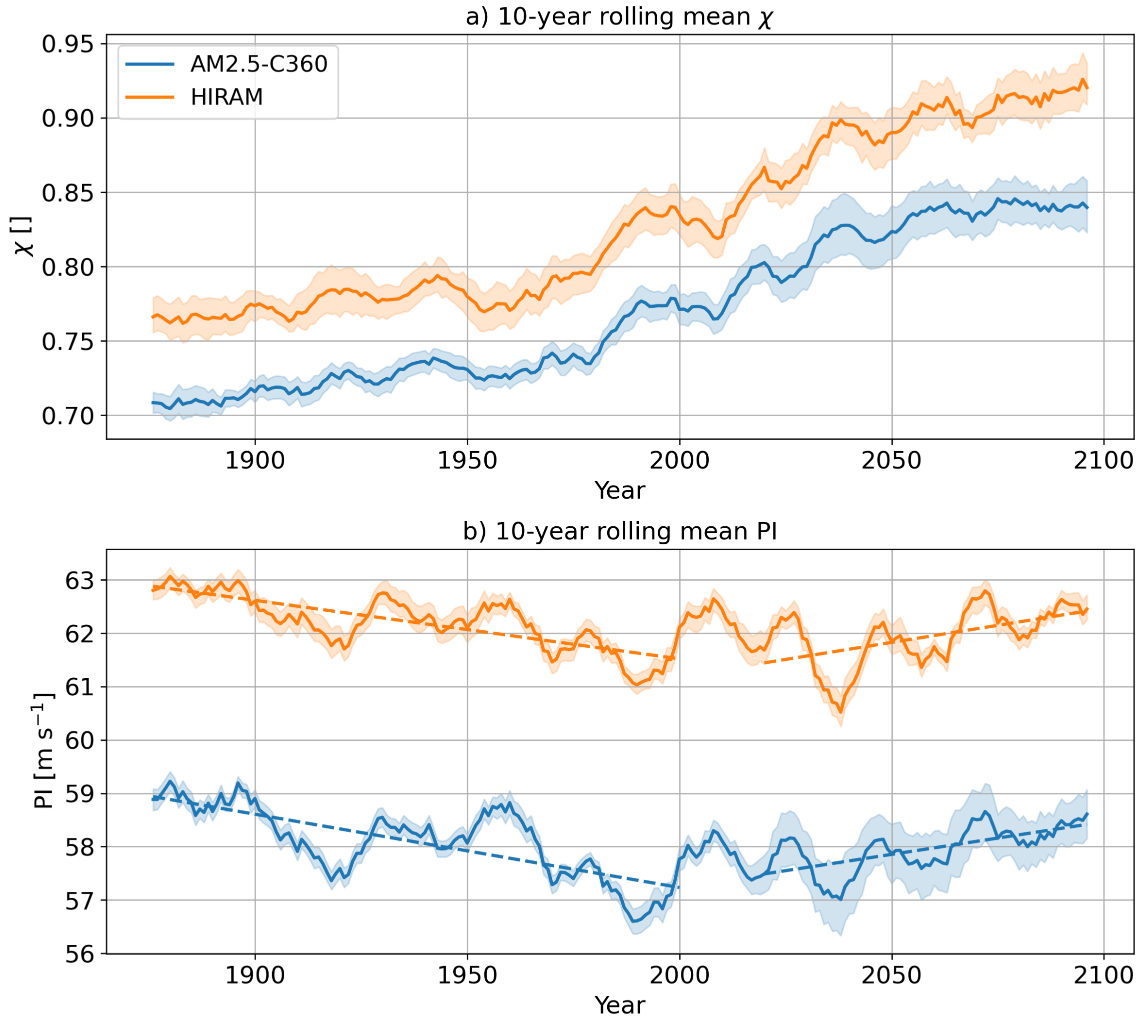

FIG. 5. Similar to Figure 3, but for the thermodynamic variables: (a) χ and (b) PI. Dotted trend lines are fitted for PI over two periods (1871–2000 and 2020–2100), showing opposite trends between these intervals in both models. Lower χ and higher PI are more favorable for TC activity.

In the present climate, Sobel et al. (2002) showed that the tropical-mean SST is closely tied to the warmest tropical SSTs. Thus, the rate at which local SSTs warm relative to the tropical-mean warming rate provides a key indicator of PI. Motivated by this framework, we compare Atlantic TC-season SST warming rates with those of the broader tropics during both the observed (Fig. 6) and projected (Fig. 7) periods. Although the tropical Atlantic warmed during the historical period (Fig. 6a), it did so more slowly than the tropical mean (Fig. 6b). In contrast, in the projected period, tropical Atlantic SSTs are expected to warm not only in absolute terms but also more rapidly than the tropical mean. These results imply that the surface-to-troposphere temperature contrast weakened in the historical record but is projected to strengthen in the future. We therefore propose that the observed decline in PI, versus its projected increase, arises from differences in relative SST changes. In particular, the spatial pattern of Atlantic SST warming relative to the tropics plays a central role in shaping PI trends and their linkage to χ, both of which are critical drivers of changes in $P(\Lambda)$.

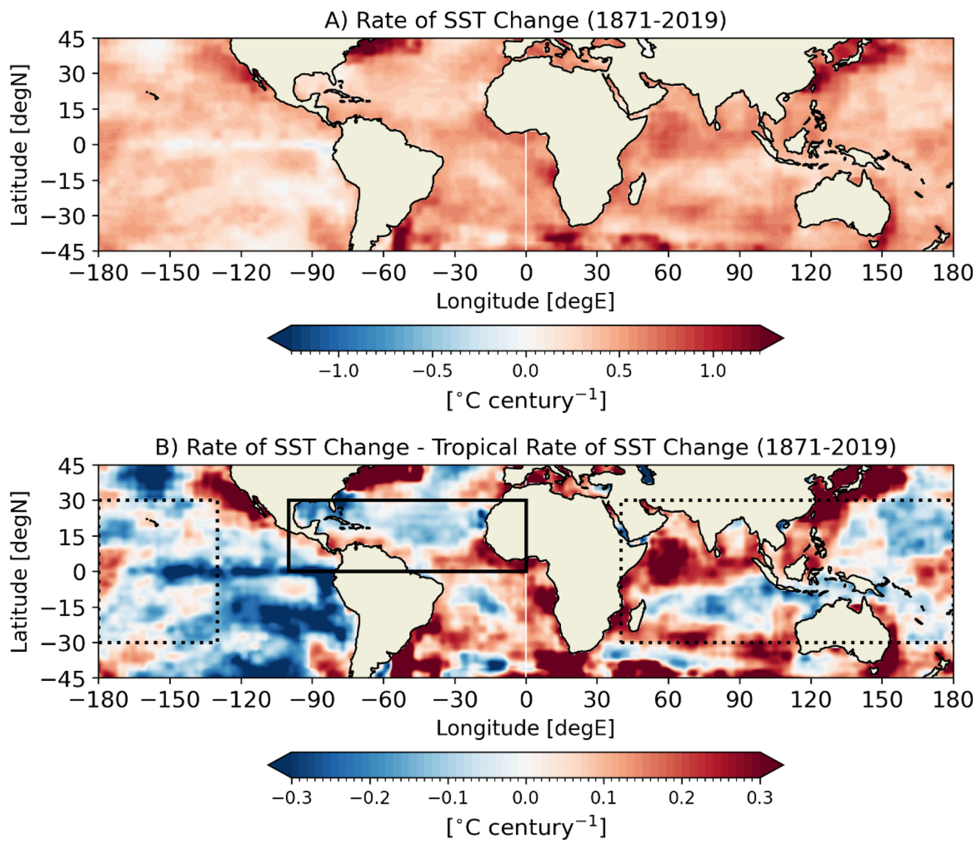

FIG. 6. (a) The rate of historical observed TC season SST changes from 1871 to 2019, with SSTs sourced from Chan et al. (2021). (b) The difference between (a) and the mean tropical TC season SST change rate over the same period. In (b), the solid black box highlights the tropical Atlantic basin, while the dotted black box marks the Indo-Pacific Warm Pool region, as defined by Weller et al. (2016), which typically encompasses the warmest ocean surface waters on Earth.

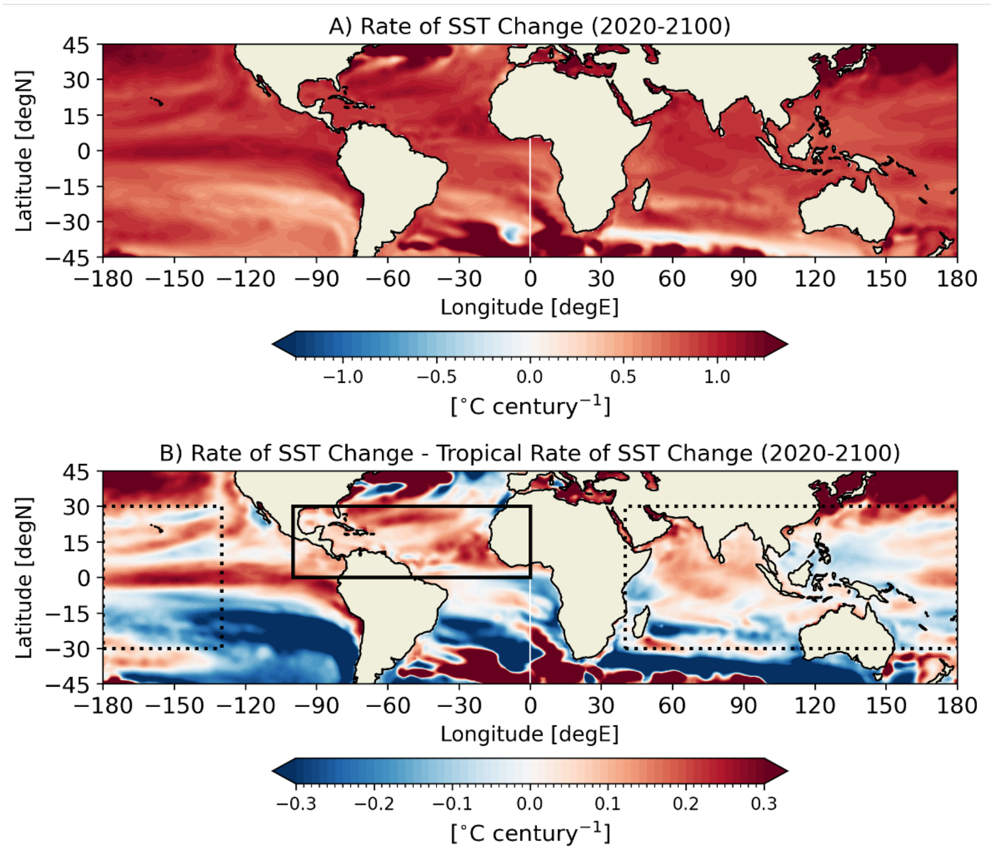

FIG. 7. Same as Fig. 6, but for the future projected period 2020–2100. Both panels are based on the ensemble mean of the 2020–2100 RCP4.5 scenario simulated by the Geophysical Fluid Dynamics Laboratory Forecast-oriented Low Ocean Resolution model, detailed in Section 2.

(ii) Dynamic variables

While the relationship between thermodynamic variables is a primary driver of the potential trend (or lack thereof) in $P(\Lambda)$, we also examine the role of the ventilation index (Eq. 6), specifically vertical wind shear, as a potential contributor to changes in $P(\Lambda)$. Figure 8b presents the time series of vertical wind shear across both models throughout the entire record. Both models simulate similar magnitudes of wind shear in the historical and projected periods. During the historical period, especially from 1950 to 2000, wind shear increases, making conditions progressively less favorable for storm activity. In contrast, the projected period shows no clear trend in wind shear: in AM2.5-C360, wind shear remains relatively stable, whereas in HIRAM, it exhibits some multidecadal variability.

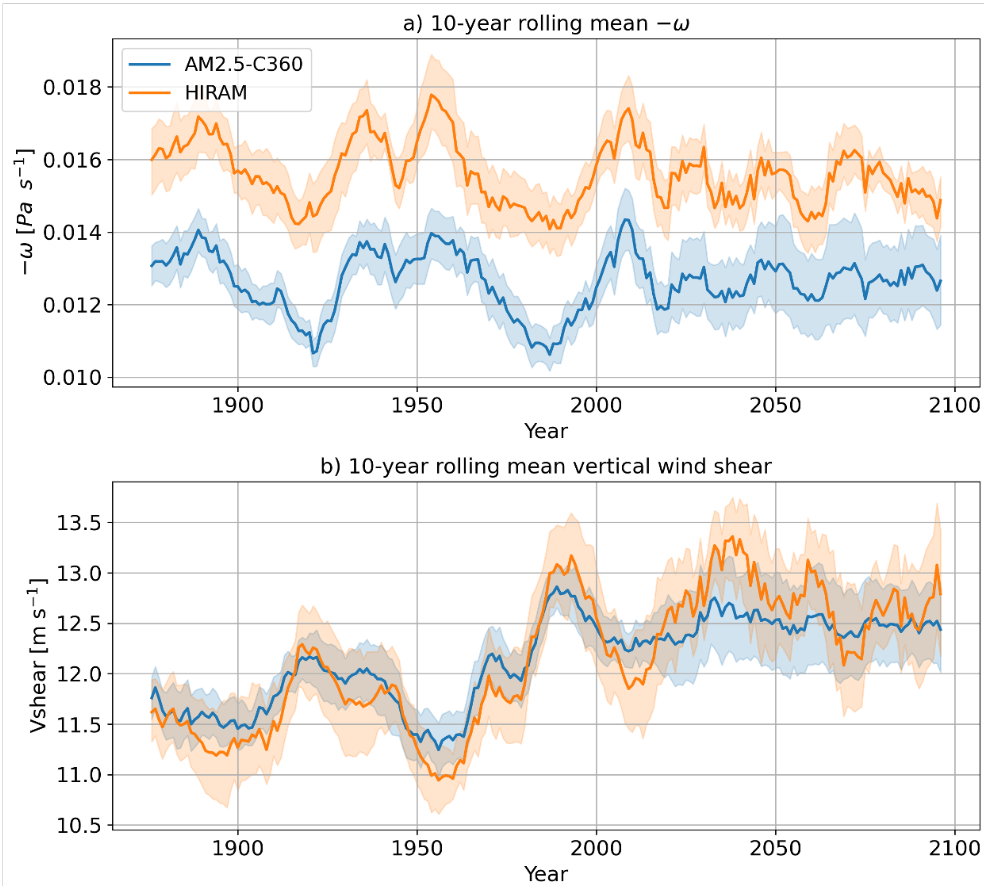

FIG. 8. Similar to Fig. 5, but for the dynamic variables: (a) $-\omega$ and (b) vertical wind shear.

The increasing wind shear during the historical period likely amplified the already declining TC favorability, as both thermodynamic and dynamic conditions became less conducive to storm development. In the projected period, however, where thermodynamic variables counterbalance each other, wind shear has the potential to influence the overall trend in $P(\Lambda)$. Yet, since wind shear remains largely stead, $P(\Lambda)$ also remains unchanged in the projected period.

To understand why vertical wind shear has increased in the tropical Atlantic TC basin throughout the historical record but is projected to remain relatively stable in the future, we analyze the zonally averaged atmospheric temperature changes across the basin (Fig. 9). Given that meridional temperature contrasts drive the thermal wind balance, we focus on temperature gradients across the tropical Atlantic. During the historical period, both models show that the equatorial Atlantic atmosphere (0–20°N) between 850 hPa and 250 hPa warms more rapidly than the subtropical Atlantic atmosphere (20–40°N) at the same altitudes (approximately 1 °C century^{-1} vs.

$0.5\ ^{\circ}C\ century^{-1}$; Fig. 9a and 9c). This enhanced warming in the equatorial region strengthens the meridional temperature gradient, which, through thermal wind balance, amplifies vertical wind shear.

In contrast, projections indicate that future warming in the equatorial Atlantic (surface to 400 hPa) will occur at a slower rate than in the subtropical Atlantic at similar heights. This reduces the poleward temperature gradient, leading to a weaker thermal wind balance and, consequently, a weakening or stabilization of vertical wind shear. These findings again highlight that spatial patterns of temperature change—rather than just the basin-wide mean warming—play a crucial role in modulating environmental factors, like wind shear, that influence TC development.

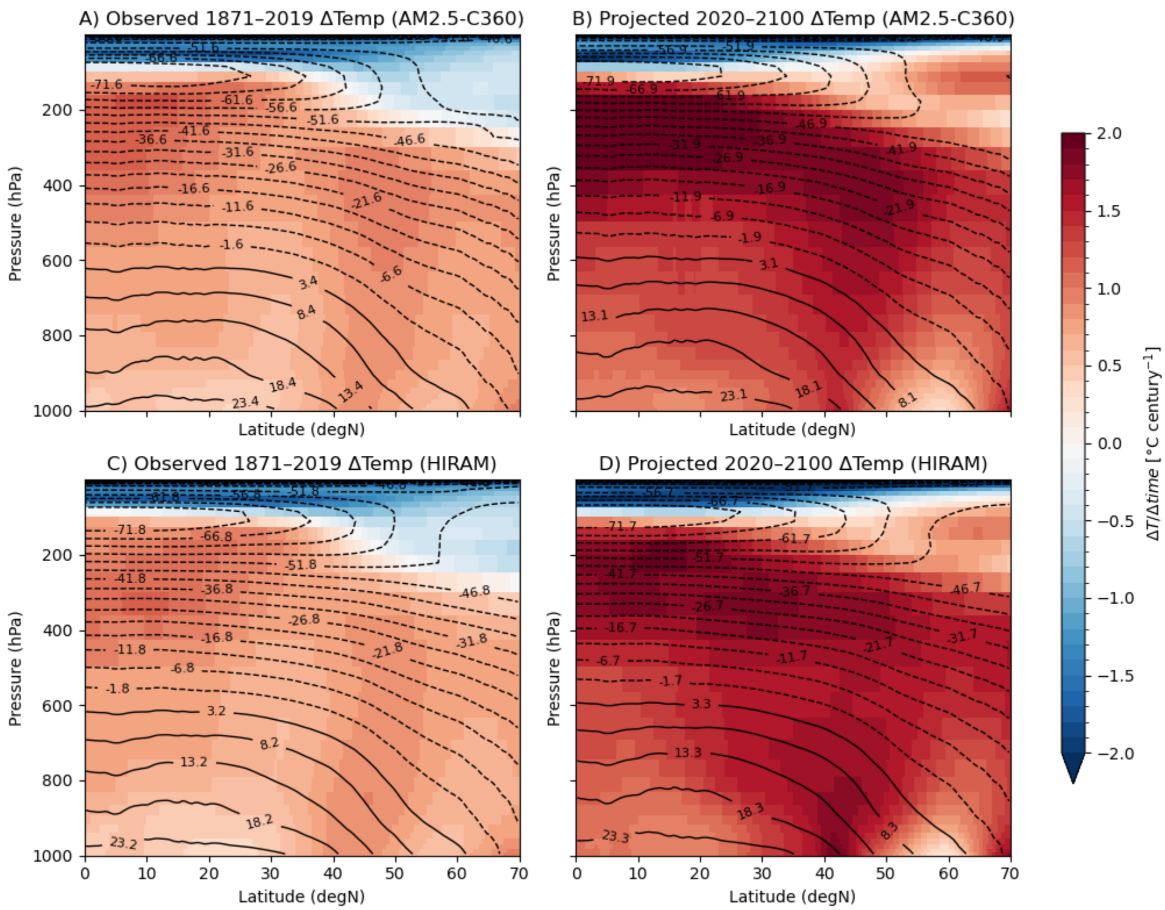

FIG. 9. Linear regression coefficients for the longitudes of the Atlantic ocean zonally-averaged cross-section of the annual TC-season atmospheric temperature change rate during: (a) the observed period of AM2.5-C360, (b) the projected period of AM2.5-C360, (c) the observed period of HIRAM, and (d) the projected period of HIRAM. Climatological temperature contours (in °C) are overlaid in black.

Next, because changes in SPI are primarily driven by variations in $-\omega$, we analyze the temporal evolution of this variable in Figure 8a. Just as SPI exhibits no clear trend across the full record in either model (Fig. 3b), $-\omega$ similarly shows no discernible long-term trend. However, both variables display pronounced multidecadal variability in the historical period, along with decadal-scale peaks and troughs in future projections. Additionally, while the typical magnitude of $-\omega$ is greater in HIRAM than in AM2.5-C360, both models exhibit comparable temporal variability. As detailed in Appendix Section b, since vorticity does not play an important role in driving TC changes, we do not include a discussion of this dynamic variable here.

4. Discussion and conclusions

As shown in Fig. 2, the TC framework of Hsieh et al. (2020) ($SPI \times P(\Lambda)$) successfully reproduces Atlantic TC variability in simulations forced with observed SSTs, as well as in projections under an RCP4.5 SST increase. Its performance is slightly stronger in HIRAM than in AM2.5-C360. Importantly, the framework achieves this skill without calibration or tuning, underscoring its ability to capture TC variability directly from local large-scale environmental conditions. This is particularly noteworthy in the Atlantic basin, where TCs frequently originate from nonlocal disturbances such as African easterly waves (AEWs; Emanuel (2022)), yet the results reinforce that local climatological conditions ultimately govern TC existence, while AEWs and other disturbances primarily set the timing and placement of genesis (Patricola and Wehner (2018)). By contrast, widely used TC proxies such as genesis potential indices (GPIs) typically require calibration before application to future scenarios (Camargo et al. 2014). Together, these findings highlight the robustness of the $SPI \times P(\Lambda)$ framework for assessing Atlantic TC variability across both historical and projected climates.

Next, we analyze how the large-scale dynamic and thermodynamic variables contribute to changes in parameterized TCs during both the historical and projected periods. Examining the temporal evolution of SPI (Fig. 3b), we find no clear long-term trend. Instead, SPI is governed by multidecadal and decadal fluctuations, largely modulated by variability in $-\omega$. In contrast, the temporal evolution of $P(\Lambda)$ is characterized by a distinct decreasing trend during the historical period, followed by a relatively stable plateau in the projected period (Fig. 3a). Notably, from 2020-2100 $P(\Lambda)$ exhibits little decadal variability, particularly in AM2.5-C360. The difference in $P(\Lambda)$'s variability between both record periods is primarily driven by the relationship between its thermodynamic components: moist entropy deficit (χ) and potential intensity (PI). During the historical period, PI and χ had a compounding effect, both becoming increasingly unfavorable for TC activity and reinforcing the decline in $P(\Lambda)$. However, in the future projection with FLOR SSTs, their opposing influences cancel out, leading to a stable $P(\Lambda)$ with no clear trend.

This shift in the thermodynamic relationship is evident in spatial analyses, where we observe a statistically significant decreasing trend in Λ during the historical period (Fig. 10), whereas no such trend is apparent in the projected period (Fig. 11). This highlights how the changing interaction between PI and χ fundamentally alters the behavior of Λ, $P(\Lambda)$, and parametrized TCs, over time.

The reversed relationship between χ and PI in the historical and projected periods stems from a shift in PI trends. While χ increases consistently throughout both records, PI decreases during the historical period but increases in the projected period. Our projected results align with previous studies (e.g., Emanuel et al. (2008), Emanuel (2021b), and Lee et al. (2020)), which similarly predict increases in both global PI and moisture deficit. However, one study using reanalysis data (Emanuel (2021a)) reports an increasing PI trend throughout the historical period, though potential biases exist in these products, particularly before the satellite era began in the 1980s.

We attribute the reversal in PI trends between the historical and projected periods to differences in the relative warming rates of the tropical Atlantic and the broader tropics, which are known to be important in modulating TC activity (Vecchi and Soden (2007); Villarini et al. (2010)). During the historical period, the tropical Atlantic warmed more slowly than the rest of the tropics, likely weakening the temperature contrast between the sea surface and the upper troposphere. Conversely, in the projected period, Atlantic SSTs are expected warm faster than the rest of the tropics, enhancing the surface-to-upper troposphere temperature contrast and fostering conditions more favorable for increases in PI and TC activity. This underscores the critical role of regional SST patterns—rather than just mean warming trends—in shaping TC activity.

These findings highlight the deep uncertainty in future TC projections (Knutson et al. 2020), a challenge that dates back to the earliest model-based study of TC frequency (Broccoli and Manabe 1990). The strong compensation between thermodynamic variables, consistent with results from downscaled CMIP6 simulations (Emanuel 2021b), suggests that these variables—directly influenced by warming—are unlikely to be the primary drivers of TC activity changes. Instead,

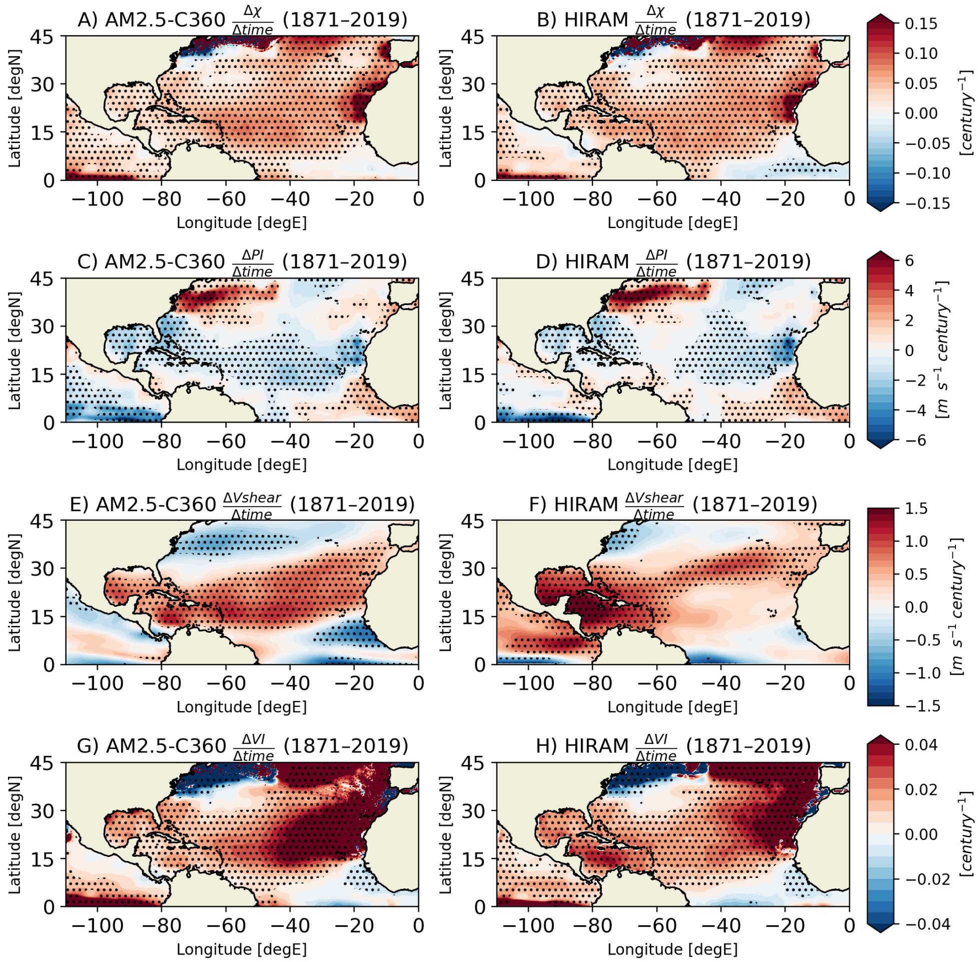

FIG. 10. Linear regression coefficients for the century-scale TC-season rate of change in (a, b) χ, (c, d) PI, (e, f) vertical wind shear, and (g,h) ventilation index (Λ) during the historical period (1871–2019) for AM2.5-C360 and HIRAM. Dotted regions indicate statistically significant trends ($p < 0.05$).

dynamic variables such as vertical wind shear, which are indirectly linked to warming through circulation changes, emerge as key determinants of future TC trends. However, because these dynamic variables are not directly constrained by warming, their future behavior remains highly uncertain (Pfahl et al. 2017).

Temperature patterns play a fundamental role in shaping both thermodynamic and dynamic variables, including wind shear and $-\omega$, through thermal wind balance and by setting the most active convective regions. Stronger meridional temperature gradients enhance vertical wind shear, while high relative SST patterns intensify deep tropical convection. Ultimately, regional SST

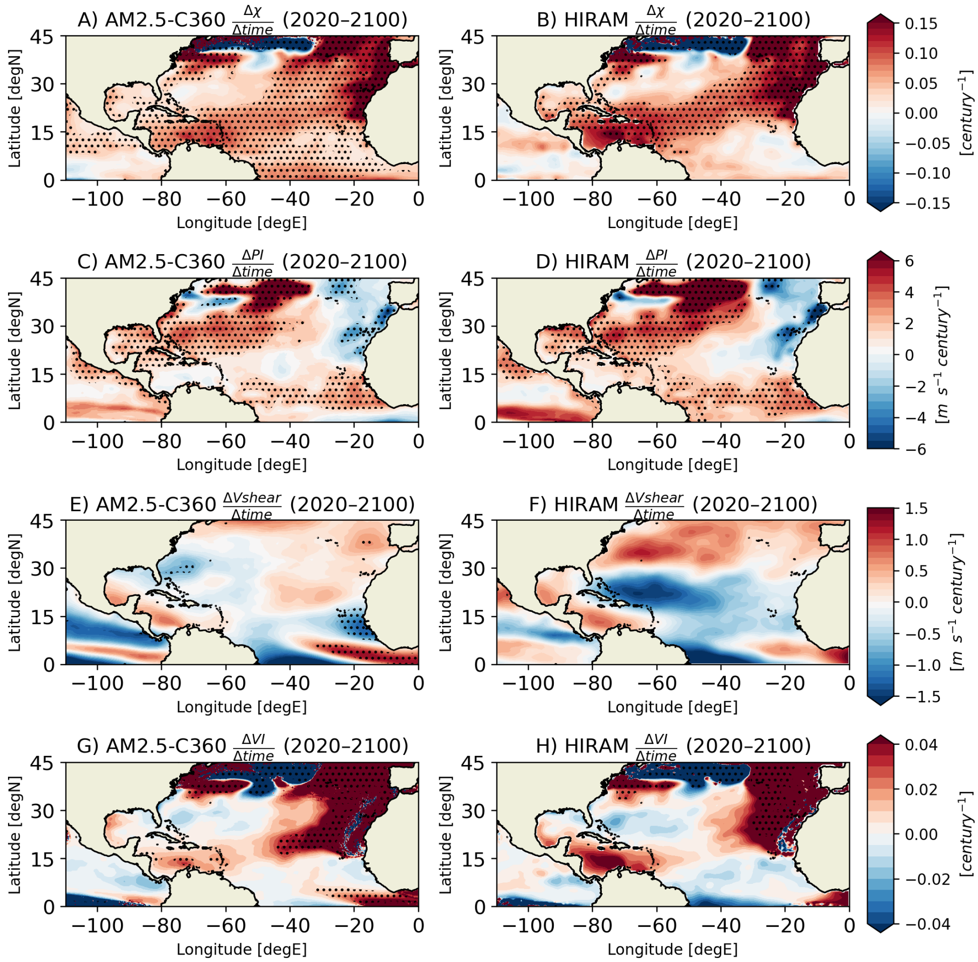

FIG. 11. Same as Fig. 10 but for the projected period (2020-2100).

patterns and the processes that control the vertical structure of warming may greatly influence changes in the dynamic variables, reinforcing the importance of spatial temperature distributions in determining future TC activity.

Building on our argument that the compensation of thermodynamic variables enables dynamic factors to influence TC activity, we observe that the trend in $P(\Lambda)$ closely mirrors that of vertical wind shear in model simulations, which is primarily determined by temperature patterns. As shown in Figure 9, vertical wind shear increases during the historical period, driven by a strengthened atmospheric meridional temperature gradient. However, these trends do not persist in future projections (Figure 11e), and substantial inter-model differences arise. For example, AM2.5-C360 forecasts a reduction in shear along the U.S. East Coast, whereas HIRAM predicts an increase in the same region. Since neither model shows a consistent basin-wide trend in shear, the projected trend in $P(\Lambda)$ remains similarly uncertain. This ambiguity in shear trends is likely due to differences in projected atmospheric temperature.

The dominant role of thermodynamic variable compensation in regulating $P(\Lambda)$ reinforces the idea that, given the uncertainty in $P(\Lambda)$ projections, future TC activity will be primarily modulated by changes in SPI, which represents the number of basin-wide seeds. This aligns with previous studies such as Hsieh et al. (2020), Vecchi et al. (2019), Sugi et al. (2020), and Yamada et al. (2021), which emphasize the critical role of TC seeds in shaping future TC activity. Our findings support this conclusion, as the projected stability of $P(\Lambda)$ (Fig. 3a) suggests that the decadal variability of parametrized TCs ($SPI \times P(\Lambda)$; Fig. 2) largely follows the variability of SPI (Fig. 3) and $-\omega$ (Fig. 8a).

While some previous studies suggest that the global number of TC seeds will decrease in a warmer climate (Hsieh et al. (2020), Vecchi et al. (2019), Sugi et al. (2020), Yamada et al. (2021)), our findings indicate that SPI, our seed proxy, does not exhibit a clear Atlantic basin-wide trend in either the historical or projected periods. Instead, SPI is characterized by decadal and multidecadal variability driven by fluctuations in $-\omega$. Although no basin-wide trends in $-\omega$ emerge, we identify localized trends within the basin, particularly along the ITCZ and within the TC main development region (Fig. 12). Specifically, an eastward shift in $-\omega$ is evident in the deep tropics, with a decreasing trend in the western basin and an increasing trend in the eastern basin, which could be as result higher rate of warming in the eastern tropical Atlantic than the western tropical Atlantic (Fig. 7b). This pattern suggests a potential eastward shift in TC genesis under warming conditions (Kortum et al. (2024)), and mirrors some observed eastward shifts in Atlantic TC tracks (Colbert and Soden 2012; Vecchi and Knutson 2011). However, significant uncertainties remain in $-\omega$, as vertical velocity and seed development could be influenced by radiative feedbacks linked to cloud processes or unresolved mechanisms, as described in the gross moist stability framework (Hsieh et al. (2023), Neelin and Held (1987)).

It is important to recognize the inter-model differences present in our results, such as variations in the framework's ability to capture TC activity in idealized simulations and discrepancies in future projections of vertical wind shear, which we suggest have to do with differences in the pattern of warming and TC seed distribution. This study examines only two atmosphere-only models, both

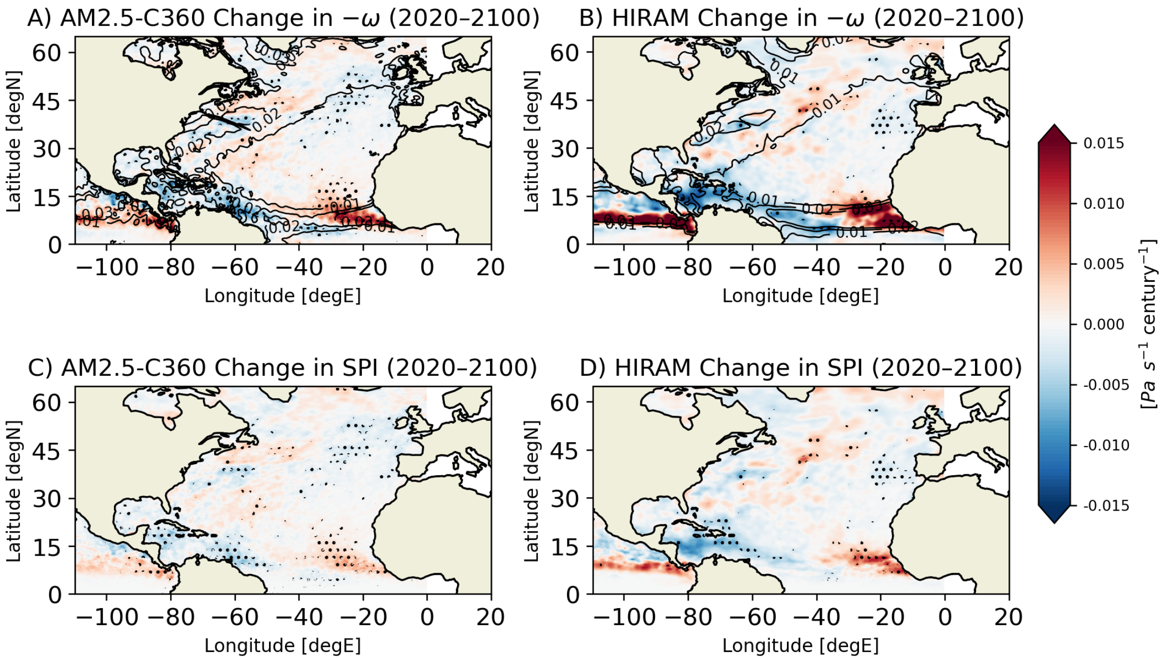

FIG. 12. Linear regression coefficients for the century-scale TC-season rate of change in (a, b) $-\omega$ and (c, d) SPI during the projected period (2020–2100) for AM2.5-C360 and HIRAM. Dotted regions indicate statistically significant trends ($p < 0.05$). In (a) and (b), black contours show the mean TC-season $-\omega$ during the historical period (1871–2019). Red (blue) shading represents regions with increasing ascent (descent) in the projection period.

of which have been shown to predict the highest number of future TCs compared to other model simulations (Bhatia et al. (2018), Hsieh et al. (2022)). However, as noted by Knutson et al. (2020), most dynamical TC-resolving models project a decrease in storm activity in a warming climate. Furthermore, because the models used here are atmosphere-only and forced exclusively by SSTs, they may highlight the limitations of relying on SSTs alone for TC predictions—an issue that became particularly evident during the 2020 TC season (Fig. 1). As suggested by Kortum et al. (2024), factors such as atmospheric chaos, aerosols, and other environmental influences could play a critical role in modulating TC activity, potentially introducing biases in SST-forced models.

Beyond the aforementioned caveats, our findings emphasize that specific SST and atmospheric spatial temperature patterns, rather than the mean warming trend, can play a pivotal role in shaping future TC activity. We find that the relationship between PI and χ is strongly influenced by the relative warming rate of the tropical Atlantic compared to the broader tropics, particularly its warmest regions Eusebi et al. (2025). Additionally, the dynamic variables are also governed by spatial temperature patterns. However, significant uncertainties remain in future SST pattern projections, especially in the Atlantic and other tropical regions, especially the Eastern Pacific (Seager et al. (2022), Shaw et al. (2024)). In the Atlantic, for instance, the extent of future AMOC weakening remains uncertain, with potential implications for Atlantic SSTs (Cheng et al. (2013), Srokosz and Bryden (2015)). To improve the reliability of future TC projections, it is essential to better constrain SST pattern projections across a wider range of climate models.

Acknowledgments. We thank Gabriele Villarini, Stephan Fueglistaler, Andrew Williams, Nadir Jeevanjee, and Hiroyuki Murakami for discussion and comments. This work has been supported in part by a grant from the Heising-Simons foundation and the Carbon Mitigation Initiative at Princeton University, funded by BP. E.L. was supported by the National Science Foundation Graduate Research Fellowship. The simulations were performed on computational resources managed and supported by Princeton Research Computing, a consortium of groups including the Princeton Institute for Computational Science and Engineering, the Office of Information Technology's High Performance Computing Center, and the Visualization Laboratory at Princeton University.

Data availability statement. Source code of the HiRAM model is available from `https://www.gfdl.noaa.gov/hiram-quickstart`. ERA5 data are available from `https://cds.climate.copernicus.eu/datasets/reanalysis-era5-pressure-levels-monthly-means?tab=overview`, and MERRA2 data are available from `https://gmao.gsfc.nasa.gov/gmao-products/merra-2/data-access_merra-2/`.

APPENDIX

Further evaluation of the seed-probability framework and its components

a. Covariance between seed and probability proxies

We assess the correlation coefficient between the annual TC-season basin-averaged SPI and $P(\Lambda)$ (Fig. A1) for both the observed historical period (1871-2019) and the projected future period (2020-2100). Our analysis reveals that, across both models and time periods, the ensemble mean of SPI and $P(\Lambda)$ exhibit a moderate correlation. Specifically, for each model, the ensemble mean correlation between the proxies is consistent across the observed and projected periods ($r \sim 0.5$ for AM2.5-C360 and $r \sim 0.7$ for HIRAM), with HIRAM generally showing stronger correlations. In AM2.5-C360, the correlation varies more widely across ensemble members, ranging from $r = 0.25$ to $r = 0.55$, while in HIRAM, the spread is narrower, with correlations ranging from $r = 0.5$ to $r = 0.7$. Despite the variation in ensemble spread and inter-model differences, it is evident that SPI and $P(\Lambda)$ are not independent, but rather covary in a manner that reflects a spatio-temporal relationship, with their combined behavior serving as a proxy for TC activity.

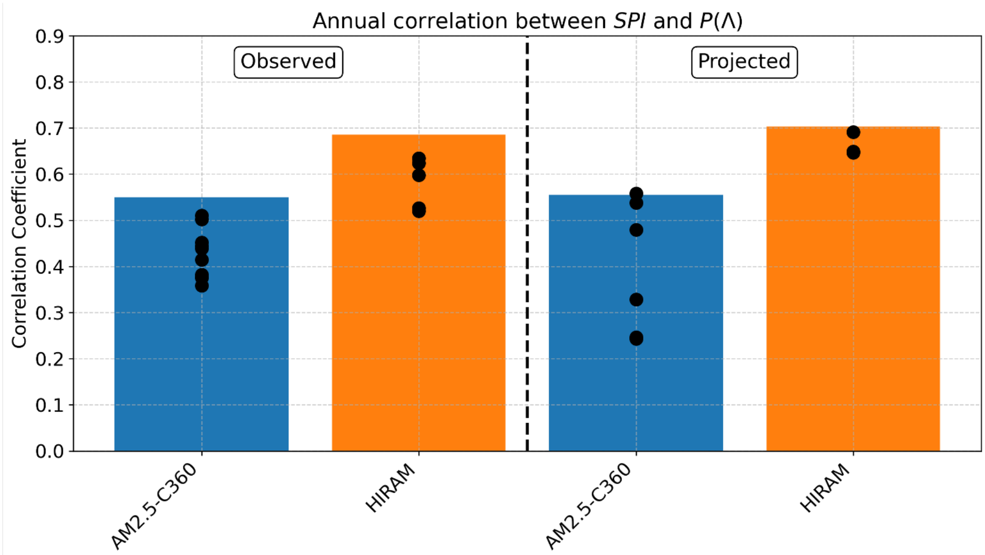

FIG. A1. Annual TC-season basin mean correlation coefficient between SPI and $P(\Lambda)$ in AM2.5-C360 (blue) and HIRAM (orange) in the *obs SST* simulation (left) and *rcp4.5 SST* simulation (right). Bars indicate the ensemble mean correlation, while black dots represent individual ensemble members.

b. Vorticity

To show that changes in the vorticity term of the SPI have a negligible impact on variations in TC activity, we perform a logarithmic decomposition of the SPI, allowing the terms to be expressed additively:

$$\begin{aligned} SPI &= \underbrace{-\omega}_{\text{vertical velocity}} \times \underbrace{\frac{1}{1+Z^{-1/0.69}}}_{\text{vorticity term } (Z_{term})} \\ &= -\omega \times Z_{term} \\ \log(SPI) &= \log(-\omega) + \log(Z_{term}). \end{aligned} \tag{A1}$$

This decomposition demonstrates that changes in $\log(SPI)$ are driven equally by additive contributions from changes in $\log(-\omega)$ and $\log(Z_{term})$. To assess these contributions over time, we analyze fluctuations in all three terms across the historical and projected record (Fig. A2). We find that $\log(Z_{term})$ exhibits minimal annual and decadal variability. Additionally, interannual and decadal variations in $\log(SPI)$ closely track those in $\log(-\omega)$, indicating that changes in SPI—and con-

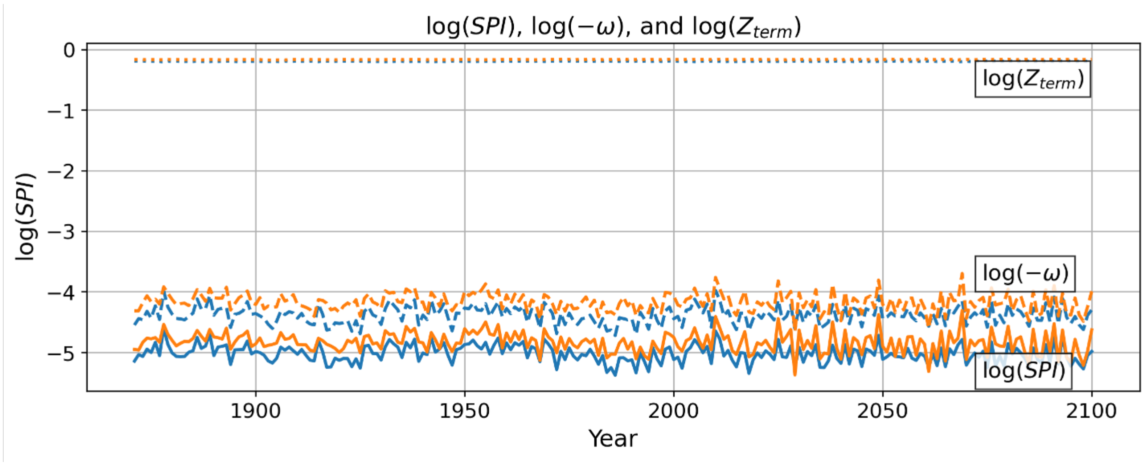

FIG. A2. Annual ensemble mean seasonally and basin-averaged $\log(SPI)$ (solid lines), $\log(-\omega)$ (dashed lines), and $\log(Z_{term})$ (dotted lines) in AM2.5-C350 (blue) and HIRAM (orange). The historical period (1871–2019) is based on the *obs SST* simulation , whereas the future period (2020–2100) is derived from the *rcp4.5 SST* simulation. These two periods are combined into a continuous time series.

sequently in parameterized TC activity—are primarily driven by fluctuations in vertical velocity rather than vorticity. Given this negligible role of vorticity, we largely disregard its influence on approximated TC activity in this report.

References

Bhatia, K., G. A. Vecchi, H. Murakami, S. Underwood, and J. P. Kossin, 2018: Projected response of tropical cyclone intensity and intensification in a global climate model. *Journal of Climate*, **31 (20)**, 8281–8298, https://doi.org/10.1175/JCLI-D-17-0898.1.

Bretherton, C. S., J. R. McCaa, and H. Grenier, 2004: A new parameterization for shallow cumulus convection and its application to marine subtropical cloud-topped boundary layers. part i: Description and 1d results. *Monthly Weather Review*, **132 (4)**, 864–882, https://doi.org/10.1175/1520-0493(2004)132⟨0864:ANPFSC⟩2.0.CO;2.

Broccoli, A. J., and S. Manabe, 1990: Can existing climate models be used to study anthropogenic changes in tropical cyclone climate? *Geophysical Research Letters*, **17 (11)**, 1917–1920, https://doi.org/10.1029/GL017i011p01917.

Bruyère, C. L., G. J. Holland, and E. Towler, 2012: Investigating the use of a genesis potential index for tropical cyclones in the north atlantic basin. *Journal of Climate*, **25 (24)**, 8611–8626, https://doi.org/10.1175/JCLI-D-11-00619.1.

Camargo, S. J., M. K. Tippett, A. H. Sobel, G. A. Vecchi, and M. Zhao, 2014: Testing the performance of tropical cyclone genesis indices in future climates using the hiram model. *Journal of Climate*, **27 (24)**, 9171–9196, https://doi.org/10.1175/JCLI-D-13-00505.1.

Camargo, S. J., and Coauthors, 2020: Characteristics of model tropical cyclone climatology and the large-scale environment. *Journal of Climate*, **33 (11)**, 4463–4483, https://doi.org/10.1175/JCLI-D-19-0500.1.

Chan, D., G. A. Vecchi, W. Yang, and P. Huybers, 2021: Improved simulation of 19th- and 20th-century north atlantic hurricane frequency after correcting historical sea surface temperatures. *Science Advances*, **7 (26)**, eabg6931, https://doi.org/10.1126/sciadv.abg6931.

Chen, J.-H., and S.-J. Lin, 2011: The remarkable predictability of interannual variability of atlantic hurricanes during the past decade. *Geophysical Research Letters*, **38 (11)**, L11 804, https://doi.org/10.1029/2011GL047629.

Cheng, W., J. C. H. Chiang, and D. Zhang, 2013: Atlantic meridional overturning circulation (AMOC) in CMIP5 models: Rcp and historical simulations. *Journal of Climate*, **26 (18)**, 7187–7198, https://doi.org/10.1175/JCLI-D-12-00496.1.

Colbert, A. J., and B. J. Soden, 2012: Climatological variations in north atlantic tropical cyclone tracks. *Journal of Climate*, **25 (2)**, 657–673, https://doi.org/10.1175/JCLI-D-11-00034.1.

Diamond, M. S., 2023: Detection of large-scale cloud microphysical changes within a major shipping corridor after implementation of the international maritime organization 2020 fuel sulfur regulations. *Atmospheric Chemistry and Physics*, **23 (14)**, 8259–8269, https://doi.org/10.5194/acp-23-8259-2023.

Emanuel, K., 2010: Tropical cyclone activity downscaled from noaa–cires reanalysis, 1908–1958. *Journal of Advances in Modeling Earth Systems*, **2 (1)**, 1–12, https://doi.org/10.3894/JAMES.2010.2.1.

Emanuel, K., 2021a: Atlantic tropical cyclones downscaled from climate reanalyses show increasing activity over past 150 years. *Nature Communications*, **12 (1)**, 7027, https://doi.org/10.1038/s41467-021-27364-8.

Emanuel, K., 2021b: Response of global tropical cyclone activity to increasing co_2: Results from downscaling cmip6 models. *Journal of Climate*, **34 (1)**, 57–70, https://doi.org/10.1175/JCLI-D-20-0367.1.

Emanuel, K., 2022: Tropical cyclone seeds, transition probabilities, and genesis. *Journal of Climate*, **35 (11)**, 3629–3643, https://doi.org/10.1175/JCLI-D-21-0922.1.

Emanuel, K., and D. Nolan, 2004: Tropical cyclone activity and global change. *Proceedings, 26th Conference on Hurricanes and Tropical Meteorology*, Miami, FL, American Meteorological Society, P2.2, URL https://ams.confex.com/ams/26HURR/techprogram/paper_75463.htm.

Emanuel, K., S. Solomon, D. Folini, S. Davis, and C. Cagnazzo, 2013: Influence of tropical tropopause layer cooling on atlantic hurricane activity. *Journal of Climate*, **26 (7)**, 2288–2303, https://doi.org/10.1175/JCLI-D-12-00242.1.

Emanuel, K., R. Sundararajan, and J. Williams, 2008: Hurricanes and global warming: Results from downscaling IPCC AR4 simulations. *Bulletin of the American Meteorological Society*, **89 (3)**, 347–367, https://doi.org/10.1175/BAMS-89-3-347.

Emanuel, K. A., 2013: Downscaling CMIP5 climate models shows increased tropical cyclone activity over the 21st century. *Proceedings of the National Academy of Sciences*, **110 (30)**, 12 219–12 224, https://doi.org/10.1073/pnas.1301293110.

Eusebi, R., W. Yang, G. A. Vecchi, and S. Fueglistaler, 2025: Statistical modeling of north atlantic hurricane frequency and the impact and role of patterned warming. *Journal of Climate*, **38 (19)**, 5391–5410, https://doi.org/10.1175/JCLI-D-24-0647.1.

Flannaghan, T. J., S. Fueglistaler, I. M. Held, S. Po-Chedley, B. Wyman, and M. Zhao, 2014: Tropical temperature trends in atmospheric general circulation model simulations and the impact of uncertainties in observed SSTs. *Journal of Geophysical Research: Atmospheres*, **119 (23)**, 13 327–13 337, https://doi.org/10.1002/2014JD022365.

Fueglistaler, S., C. Radley, and I. M. Held, 2015: The distribution of precipitation and the spread in tropical upper tropospheric temperature trends in CMIP5/AMIP simulations. *Geophysical Research Letters*, **42 (14)**, 6000–6007, https://doi.org/10.1002/2015GL064966.

Gelaro, R., and Coauthors, 2017: The modern-era retrospective analysis for research and applications, version 2 (MERRA-2). *Journal of Climate*, **30 (14)**, 5419–5454, https://doi.org/10.1175/JCLI-D-16-0758.1.

Goldenberg, S. B., C. W. Landsea, A. M. Mestas-Nuñez, and W. M. Gray, 2001: The recent increase in atlantic hurricane activity: Causes and implications. *Science*, **293 (5529)**, 474–479, https://doi.org/10.1126/science.1060040.

Harris, L. M., S.-J. Lin, and C. Tu, 2016: High-resolution climate simulations using GFDL HiRAM with a stretched global grid. *Journal of Climate*, **29 (11)**, 4293–4314, https://doi.org/10.1175/JCLI-D-15-0389.1.

Held, I. M., and B. J. Soden, 2000: Water vapor feedback and global warming. *Annual Review of Environment and Resources*, **25**, 441–475, https://doi.org/10.1146/annurev.energy.25.1.441.

Hersbach, H., and Coauthors, 2020: The ERA5 global reanalysis. *Quarterly Journal of the Royal Meteorological Society*, **146 (730)**, 1999–2049, https://doi.org/10.1002/qj.3803.

Hsieh, T.-L., G. A. Vecchi, W. Yang, I. M. Held, and S. T. Garner, 2020: Large-scale control on the frequency of tropical cyclones and seeds: a consistent relationship across a hierarchy of global atmospheric models. *Climate Dynamics*, **55 (11)**, 3177–3196, https://doi.org/10.1007/s00382-020-05446-5.

Hsieh, T.-L., W. Yang, G. A. Vecchi, and M. Zhao, 2022: Model spread in the tropical cyclone frequency and seed propensity index across global warming and enso-like perturbations. *Geophysical Research Letters*, **49 (7)**, e2021GL097 157, https://doi.org/10.1029/2021GL097157.

Hsieh, T.-L., B. Zhang, W. Yang, G. A. Vecchi, M. Zhao, B. J. Soden, and C. Wang, 2023: The influence of large-scale radiation anomalies on tropical cyclone frequency. *Journal of Climate*, **36 (16)**, 5431–5441, https://doi.org/10.1175/JCLI-D-22-0449.1.

Ikehata, K., and M. Satoh, 2021: Climatology of tropical cyclone seed frequency and survival rate in tropical cyclones. *Geophysical Research Letters*, **48 (18)**, e2021GL093 626, https://doi.org/10.1029/2021GL093626.

Jordan, G., and M. Henry, 2024: IMO2020 regulations accelerate global warming by up to 3 years in UKESM1. *Earth's Future*, **12 (8)**, e2024EF005 011, https://doi.org/10.1029/2024EF005011.

Klotzbach, P. J., 2011a: El niño–southern oscillation's impact on atlantic basin hurricanes and u.s. landfalls. *Journal of Climate*, **24 (4)**, 1252–1263, https://doi.org/10.1175/2010JCLI3799.1.

Klotzbach, P. J., 2011b: The influence of el niño–southern oscillation and the atlantic multidecadal oscillation on caribbean tropical cyclone activity. *Journal of Climate*, **24 (3)**, 721–731, https://doi.org/10.1175/2010JCLI3705.1.

Klotzbach, P. J., S. G. Bowen, R. Pielke, and M. Bell, 2018: Continental u.s. hurricane landfall frequency and associated damage: Observations and future risks. *Bulletin of the American Meteorological Society*, **99 (7)**, 1359–1376, https://doi.org/10.1175/BAMS-D-17-0184.1.

Klotzbach, P. J., K. M. Wood, C. J. Schreck III, S. G. Bowen, C. M. Patricola, and M. M. Bell, 2022: Trends in global tropical cyclone activity: 1990–2021. *Geophysical Research Letters*, **49 (6)**, e2021GL095 774, https://doi.org/10.1029/2021GL095774.

Knutson, T., and Coauthors, 2020: Tropical cyclones and climate change assessment: Part II: Projected response to anthropogenic warming. *Bulletin of the American Meteorological Society*, **101 (3)**, E303–E322, https://doi.org/10.1175/BAMS-D-18-0194.1.

Kortum, G., G. A. Vecchi, T.-L. Hsieh, and W. Yang, 2024: Influence of weather and climate on multidecadal trends in atlantic hurricane genesis and tracks. *Journal of Climate*, **37 (5)**, 1501–1522, https://doi.org/10.1175/JCLI-D-23-0088.1.

Lee, C.-Y., S. J. Camargo, A. H. Sobel, and M. K. Tippett, 2020: Statistical–dynamical downscaling projections of tropical cyclone activity in a warming climate: Two diverging genesis scenarios. *Journal of Climate*, **33 (11)**, 4201–4221, https://doi.org/10.1175/JCLI-D-19-0452.1.

Lee, C.-Y., A. H. Sobel, M. K. Tippett, S. J. Camargo, M. Wüest, M. Wehner, and H. Murakami, 2023: Climate change signal in atlantic tropical cyclones today and near future. *Earth's Future*, **11 (11)**, e2023EF003 539, https://doi.org/10.1029/2023EF003539.

Manganello, J. V., and Coauthors, 2012: Tropical cyclone climatology in a 10-km global atmospheric gcm: Toward weather-resolving climate modeling. *Journal of Climate*, **25 (11)**, 3867–3893, https://doi.org/10.1175/JCLI-D-11-00346.1.

Murakami, H., and B. Wang, 2022: Patterns and frequency of projected future tropical cyclone genesis are governed by dynamic effects. *Communications Earth & Environment*, **3 (1)**, 1–10, https://doi.org/10.1038/s43247-022-00410-z.

Neelin, J. D., and I. M. Held, 1987: Modeling tropical convergence based on the moist static energy budget. *Monthly Weather Review*, **115 (1)**, 3–12, https://doi.org/10.1175/1520-0493(1987)115⟨0003:MTCBOT⟩2.0.CO;2.

Olszewski, K., 1986: Saturation deficit in various air masses. *Miscellanea Geographica*, **2 (1)**, 79–84, https://doi.org/10.2478/mgrsd-1986-020111.

Patricola, C. M., P. Chang, and R. Saravanan, 2016: Degree of simulated suppression of atlantic tropical cyclones modulated by flavour of el niño. *Nature Geoscience*, **9 (2)**, 155–160, https://doi.org/10.1038/ngeo2624.

Patricola, C. M., R. Saravanan, and P. Chang, 2018: The response of atlantic tropical cyclones to suppression of african easterly waves. *Geophysical Research Letters*, **45 (1)**, 471–479, https://doi.org/10.1002/2017GL076081.

Patricola, C. M., and M. F. Wehner, 2018: Anthropogenic influences on major tropical cyclone events. *Nature*, **563 (7731)**, 339–346, https://doi.org/10.1038/s41586-018-0673-2.

Pfahl, S., P. A. O'Gorman, and E. M. Fischer, 2017: Understanding the regional pattern of projected future changes in extreme precipitation. *Nature Climate Change*, **7 (6)**, 423–427, https://doi.org/10.1038/nclimate3287.

Pielke, R. A., and C. N. Landsea, 1999: La niña, el niño, and atlantic hurricane damages in the united states. *Bulletin of the American Meteorological Society*, **80 (10)**, 2027–2033.

Ramsay, H. A., and A. H. Sobel, 2011: Effects of relative and absolute sea surface temperature on tropical cyclone potential intensity using a single-column model. *Journal of Climate*, **24 (1)**, 183–193, https://doi.org/10.1175/2010JCLI3690.1.

Ritchie, E. A., and G. J. Holland, 1999: Large-scale patterns associated with tropical cyclogenesis in the western pacific. *Monthly Weather Review*, **127 (9)**, 2027–2043, https://doi.org/10.1175/1520-0493(1999)127⟨2027:LSPAWT⟩2.0.CO;2.

Seager, R., N. Henderson, and M. Cane, 2022: Persistent discrepancies between observed and modeled trends in the tropical pacific ocean. *Journal of Climate*, **35 (14)**, 4571–4584, https://doi.org/10.1175/JCLID210648.1.

Shaw, T. A., and Coauthors, 2024: Regional climate change: consensus, discrepancies, and ways forward. *Frontiers in Climate*, **6**, 1–14, https://doi.org/10.3389/fclim.2024.1391634.

Sobel, A. H., I. M. Held, and C. S. Bretherton, 2002: The enso signal in tropical tropospheric temperature. *Journal of Climate*, **15 (18)**, 2702–2708, https://doi.org/10.1175/1520-0442(2002)015⟨2702:TESITT⟩2.0.CO;2.

Sobel, A. H., A. A. Wing, S. J. Camargo, C. M. Patricola, G. A. Vecchi, C. Lee, and M. K. Tippett, 2021: Tropical cyclone frequency. *Earth's Future*, **9 (12)**, e2021EF002 275, https://doi.org/10.1029/2021EF002275.

Srokosz, M., and H. Bryden, 2015: Observing the atlantic meridional overturning circulation yields a decade of inevitable surprises. *Science*, **348 (6241)**, 1255 575, https://doi.org/10.1126/science.1255575.

Sugi, M., Y. Yamada, K. Yoshida, R. Mizuta, M. Nakano, C. Kodama, and M. Satoh, 2020: Future changes in the global frequency of tropical cyclone seeds. *SOLA*, **16**, 70-74, https://doi.org/10.2151/sola.2020012.

Tang, B., and S. J. Camargo, 2014: Environmental control of tropical cyclones in cmip5: A ventilation perspective. *Journal of Advances in Modeling Earth Systems*, **6 (1)**, 115-128, https://doi.org/10.1002/2013MS000294.

Tang, B., and K. Emanuel, 2010: Midlevel ventilation's constraint on tropical cyclone intensity. *Journal of the Atmospheric Sciences*, **67 (6)**, 1817-1830, https://doi.org/10.1175/2010JAS3318.1.

Tang, B., and K. Emanuel, 2012: A ventilation index for tropical cyclones. *Bulletin of the American Meteorological Society*, **93 (12)**, 1901-1915, https://doi.org/10.1175/BAMSD1100165.1.

Tippett, M., S. Camargo, and A. Sobel, 2011: A poisson regression index for tropical cyclone genesis and the role of large-scale vorticity in genesis. *Journal of Climate*, **24 (9)**, 2335-2357, https://doi.org/10.1175/2010JCLI3811.1.

Vecchi, G. A., S. Fueglistaler, I. M. Held, T. R. Knutson, and M. Zhao, 2013: Impacts of atmospheric temperature trends on tropical cyclone activity. *Journal of Climate*, **26 (11)**, 3877–3898, https://doi.org/10.1175/JCLI-D-12-00503.1.

Vecchi, G. A., and T. R. Knutson, 2008: On estimates of historical north atlantic tropical cyclone activity. *Journal of Climate*, **21 (14)**, 3580–3600, https://doi.org/10.1175/2008JCLI2178.1.

Vecchi, G. A., and T. R. Knutson, 2011: Estimating annual numbers of atlantic hurricanes missing from the hurdat database (1878–1965) using ship track density. *Journal of Climate*, **24 (6)**, 1736–1746, https://doi.org/10.1175/2010JCLI3810.1.

Vecchi, G. A., C. Landsea, W. Zhang, G. Villarini, and T. Knutson, 2021: Changes in atlantic major hurricane frequency since the late-19th century. *Nature Communications*, **12 (1)**, 4054, https://doi.org/10.1038/s41467-021-24268-5.

Vecchi, G. A., and B. J. Soden, 2007: Effect of remote sea surface temperature change on tropical cyclone potential intensity. *Nature*, **450 (7172)**, 1066–1070, https://doi.org/10.1038/nature06423.

Vecchi, G. A., and Coauthors, 2014: On the seasonal forecasting of regional tropical cyclone activity. *Journal of Climate*, **27 (21)**, 8065–8087, https://doi.org/10.1175/JCLI-D-14-00158.1.

Vecchi, G. A., and Coauthors, 2019: Tropical cyclone sensitivities to co2 doubling: roles of atmospheric resolution, synoptic variability and background climate changes. *Climate Dynamics*, **53 (9)**, 5999–6033, https://doi.org/10.1007/s00382-019-04913-y.

Villarini, G., G. A. Vecchi, T. R. Knutson, and J. A. Smith, 2011a: Is the recorded increase in short-duration north atlantic tropical storms spurious? *Journal of Geophysical Research: Atmospheres*, **116**, D10 112, https://doi.org/10.1029/2010JD015493.

Villarini, G., G. A. Vecchi, T. R. Knutson, M. Zhao, and J. A. Smith, 2011b: North atlantic tropical storm frequency response to anthropogenic forcing: Projections and sources of uncertainty. *Journal of Climate*, **24 (13)**, 3224–3248, https://doi.org/10.1175/2011JCLI3853.1.

Villarini, G., G. A. Vecchi, and J. A. Smith, 2010: Modeling the dependence of tropical storm counts in the north atlantic basin on climate indices. *Monthly Weather Review*, **138 (7)**, 2681–2705, https://doi.org/10.1175/2010MWR3315.1.

Walsh, K. J. E., S. J. Camargo, T. R. Knutson, J. Kossin, T.-C. Lee, H. Murakami, and C. Patricola, 2019: Tropical cyclones and climate change. *Tropical Cyclone Research and Review*, **8 (4)**, 240–250, https://doi.org/10.1016/j.tcrr.2020.01.004.

Wang, B., and H. Murakami, 2020: Dynamic genesis potential index for diagnosing present-day and future global tropical cyclone genesis. *Environmental Research Letters*, **15 (11)**, 114 008, https://doi.org/10.1088/1748-9326/abbb01.

Weller, E., S.-K. Min, W. Cai, F. W. Zwiers, Y.-H. Kim, and D. Lee, 2016: Human-caused indo-pacific warm pool expansion. *Science Advances*, **2 (7)**, e1501 719, https://doi.org/10.1126/sciadv.1501719.

Xie, L., T. Yan, L. J. Pietrafesa, J. M. Morrison, and T. Karl, 2005: Climatology and interannual variability of north atlantic hurricane tracks. *Journal of Climate*, **18 (24)**, 5370–5381, https://doi.org/10.1175/JCLI3560.1.

Yamada, Y., and Coauthors, 2021: Evaluation of the contribution of tropical cyclone seeds to changes in tropical cyclone frequency due to global warming in high-resolution multi-model ensemble simulations. *Progress in Earth and Planetary Science*, **8 (1)**, 11, https://doi.org/10.1186/s40645-020-00397-1.

Yang, W., T.-L. Hsieh, and G. A. Vecchi, 2021: Hurricane annual cycle controlled by both seeds and genesis probability. *Proceedings of the National Academy of Sciences*, **118 (41)**, e2108397 118, https://doi.org/10.1073/pnas.2108397118.

Zhang, B., B. J. Soden, G. A. Vecchi, and W. Yang, 2021: The role of radiative interactions in tropical cyclone development under realistic boundary conditions. *Journal of Climate*, **34 (6)**, 2079–2091, https://doi.org/10.1175/JCLI-D-20-0574.1.

Zhang, C., 1993: Large-scale variability of atmospheric deep convection in relation to sea surface temperature in the tropics. *Journal of Climate*, **6 (10)**, 1898–1913, https://doi.org/10.1175/1520-0442(1993)006⟨1898:LSVOAD⟩2.0.CO;2.

Zhang, J., Y.-S. Chen, E. Gryspeerdt, T. Yamaguchi, and G. Feingold, 2025: Radiative forcing from the 2020 shipping fuel regulation is large but hard to detect. *Communications Earth & Environment*, **6 (1)**, 1–11, https://doi.org/10.1038/s43247-024-01911-9.

Zhang, R., and T. L. Delworth, 2006: Impact of atlantic multidecadal oscillations on india/sahel rainfall and atlantic hurricanes. *Geophysical Research Letters*, **33 (17)**, L17 712, https://doi.org/10.1029/2006GL026267.

Zhao, M., and I. M. Held, 2010: An analysis of the effect of global warming on the intensity of atlantic hurricanes using a gcm with statistical refinement. *Journal of Climate*, **23 (23)**, 6382–6395, https://doi.org/10.1175/2010JCLI3837.1.

Zhao, M., I. M. Held, S.-J. Lin, and G. A. Vecchi, 2009: Simulations of global hurricane climatology, interannual variability, and response to global warming using a 50-km resolution gcm. *Journal of Climate*, **22 (24)**, 6653–6678, https://doi.org/10.1175/2009JCLI3049.1.